Journal of Experimental Biology and Agricultural Sciences, December - 2024; Volume – 12(6) page 800 – 828

Journal of Experimental Biology and Agricultural Sciences

http://www.jebas.org

ISSN No. 2320 – 8694

In silico Analysis of Natural Iridoids as Primary Amoebic Meningoencephalitis Inhibitors: Molecular Docking, MD Simulation, MMPBSA, and DFT Analyses

Prinsa[1], Supriyo Saha[2*]

[1]Department of Pharmaceutical Chemistry, Siddhartha Institute of Pharmacy, Near IT-Park, Sahastradhara Road, Dehradun 248001, Uttarakhand, India
[2]Department of Pharmaceutical Chemistry, Uttaranchal Institute of Pharmaceutical Sciences, Uttaranchal University, Dehradun-248001, Uttarakhand, India

Received – August 29, 2024; Revision – December 12, 2024; Accepted – December 21, 2024
Available Online – January 15, 2025

DOI: http://dx.doi.org/10.18006/2024.12(6).800.828

KEYWORDS

Primary Amoebic Meningoencephalitis (PAM)

Iridoids

Molecular Docking

MD Simulation

MMPBSA

DFT

ABSTRACT

Iridoids have demonstrated various activities, including anti-inflammatory, anticancer, cardioprotective, antiviral, hepatoprotective, antihyperglycemic, and antiparasitic effects. The brain-eating amoeba *Naegleria fowleri* is responsible for primary amoebic meningoencephalitis, a brain inflammation. In this study, 52 iridoids were selected through an extensive literature survey, and 22 of these iridoids passed the drug-likeness filter. The selected iridoids were molecularly docked against the *N. fowleri* CYP51 receptor, using voriconazole as a standard for comparison. The docking score for voriconazole was -7.6 kcal/mol, while the scores for 10-isovaleroyl-dihydropenstemide and Patrinalloside A were -8.9 and -8.6 kcal/mol, respectively. According to molecular dynamics (MD) simulation data, the interacting amino acid residues exhibited fluctuations within a specific range, with the Root Mean Square Deviation (RMSD) values stabilizing throughout the experiment. When interacting with the receptor linked to amoebic meningoencephalitis, 10-isovaleroyl-dihydropenstemide and Patrinalloside A showed free binding energies of -71.922 kJ/mol and -61.243 kJ/mol, respectively, based on Molecular Mechanics Poisson-Boltzmann Surface Area (MMPBSA) calculations. Furthermore, Fragment Molecular Orbital (FMO) and Molecular Electrostatic Potential (MEP) analyses of 10-isovaleroyl-dihydropenstemide and Patrinalloside A revealed potential nucleophilic-electrophilic attack zones, indicating they are chemically reactive. The analysis of both compounds' ADMET (Absorption, Distribution, Metabolism, Excretion, and Toxicity) indicated non-toxic behaviour. These findings suggest that natural iridoids have significant potential in combating primary amoebic meningoencephalitis.

* Corresponding author
E-mail: supriyo9@gmail.com (Supriyo Saha)

Peer review under responsibility of Journal of Experimental Biology and Agricultural Sciences.

Production and Hosting by Horizon Publisher India [HPI] (http://www.horizonpublisherindia.in/).
All rights reserved.

All the articles published by Journal of Experimental Biology and Agricultural Sciences are licensed under a Creative Commons Attribution-NonCommercial 4.0 International License Based on a work at www.jebas.org.

1 Introduction

Thermophilic amoeba is responsible for amoebic encephalitis, a central nervous system infection. This condition has two forms: granulomatous amoebic encephalitis and primary amoebic meningoencephalitis (PAM) (Güémez and García 2021). The amoeba species primarily responsible for spreading the infection include *Naegleria*, *Acanthamoeba*, *Sappinia*, and *Balamuthia*. These microorganisms thrive in tropical regions and are commonly found in freshwater bodies such as lakes and ponds (Rojo et al. 2023). Among these, *N. fowleri*, a species of *Naegleria*, directly infects the central nervous system and damages brain cells associated with PAM. The flagellate form of *N. fowleri* has also been detected in human cerebrospinal fluid (Cooper et al. 2019). Transmission to the central nervous system results in brain edema, inflammation, and loss of brain tissue. Trophozoites of *N. fowleri* penetrate the olfactory mucosa to reach the olfactory bulb, leading to inflammation and parenchymal damage as they cross the cribriform plate. This deadly infection earns *N. fowleri* the nickname "brain-eating amoeba." Although rare, this infection is lethal, and the chances of survival depend on early detection and treatment (Calis et al. 2020). Despite current antimicrobial therapies, the mortality rate remains approximately 90%. Recently reported cases of brain-eating amoeba in India and other countries have underscored the need to re-emphasize the significance of primary amoebic meningoencephalitis and explore possible cures and treatments (Wang et al. 2020).

Iridoid compounds, classified as cyclopentane pyran monoterpenes, possess several medicinal properties. Depending on their chemical structure, iridoids can be categorized into four groups: iridoid glycosides, secoiridoid glycosides, non-glycosidic iridoids, and bis-iridoids (Grover et al. 2023). These compounds have been employed in traditional medicine for liver protection (Zhang et al. 2024), inflammation reduction (He et al. 2023), and promoting wound healing (Geng et al. 2024). Researchers have discovered that iridoids are crucial in inhibiting and controlling the growth of a wide range of pathogenic microorganisms (Shi et al. 2023; Schou et al. 2024). Several iridoids, including 10-Isovaleroyl-dihydropenstemide, brasoside, Patrinalloside A, Polystachyn A, and Asperuloside, are widely cultivated for their various health benefits, such as anti-inflammatory, neuroprotective, hepatoprotective, anti-tumorigenic, antiviral, anti-malarial, and anti-protozoal effects. This pharmacological potential suggests that these iridoids could effectively manage protozoal infections such as PAM (Zhang et al. 2023). This research focuses on repurposing natural iridoids to manage primary amoebic meningoencephalitis through molecular docking, molecular dynamic simulations, and density functional theory analysis. The goal is to identify the most promising iridoid to combat this lethal brain infection.

2 Materials and Methods

2.1 Collection of Data and Assessment Drug Likeness Parameter

A total of 52 iridoids were identified through an extensive literature search, and their drug-likeness parameters were evaluated according to the Lipinski Rule of Five. According to this rule, the partition coefficient should not exceed five, the number of hydrogen bond donors should be no more than five, and the number of hydrogen bond acceptors should not exceed ten (Daina et al., 2017). The drug-likeness parameter was used as a primary filter in the drug development process (Table 1). Out of the 52 iridoids, 30 did not pass this primary filter (Chen et al., 2020). As a result, 22 iridoids were selected for further studies, including molecular docking, molecular dynamics simulation, and quantum mechanics-based electronic nature analysis, targeting the CYP51 receptor of *N. fowleri*.

2.2 Molecular Docking Study using AutoDock Vina

2.2.1 Preparation of protein

This research examined the CYP51 receptor of *Naegleria fowleri* complexed with itraconazole (PDB ID: 6AYC). The structural characteristics of the receptor were analyzed using a Ramachandran plot. Additionally, the presence of non-bonded interactions among various atom types within the receptor was assessed based on the ERRAT score. The three-dimensional structural classification of the protein, which includes alpha helices, beta sheets, and loops, was also determined using VERIFY 3D.

2.2.2 Preparation of iridoids structures for molecular docking

Avogadro software was utilized to draw structures and perform force field-based energy minimization on selected iridoids and the standard compound voriconazole (Hanwell et al. 2012). All structures were saved in PDB format, and using AutoDock Tools 1.5.6, they were converted into docking-compatible PDBQT format. The Drug Discovery Studio Visualizer was employed to examine protein-ligand interactions. The grid box dimensions for the *N. fowleri* CYP51 protein were 14.088, -4.933, and 13.271 along the x, y, and z axes. The root mean square deviation (RMSD) value between the redocked and unprocessed crystallographic conformations was less than 1.25 Å. This information supports the validity and reliability of the docking process (Goodsell et al. 2021).

2.3 Molecular Dynamic (MD) Simulation of the selected iridoids

To visualize the atomic-level interaction patterns of a ligand molecule within a receptor in the presence of solvent, ions, temperature, and pressure, molecular dynamics (MD) simulations

Table 1 List of irdoids with chemical structure, biological source, bioactivities and drug likeness parameter

S.N.	Name of the Molecules	Structure	Biological Source	Activities	Lipinski rule
1	6-O-Alpha-D-galactopyranosylharpagoside	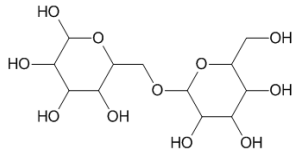	*Harpagophytum procumbens*	Anti- inflammatory	Rejected
2	6'-O-Sinapoyl-geniposide	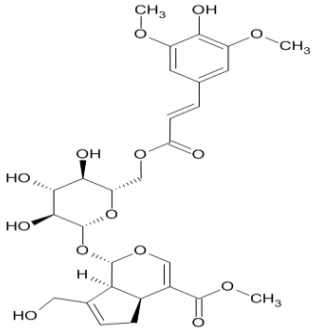	*Gardenia jasminoides*	Anti- inflammatory, Antioxidant, Anti diabetic, Hepatoprotective, Neuroprotective	Rejected
3	6-O-Trans-cinnamoyl-secologanoside	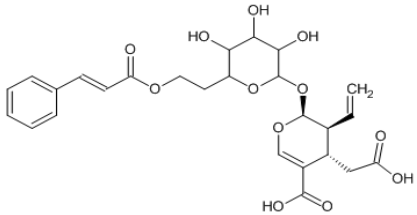	*Ligustrum lucidum*	Osteogenic activity	Rejected
4	6'-O-Trans-para-coumaroylgeniposide	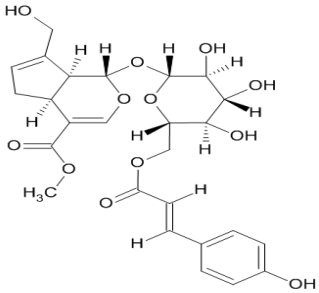	*Rubiaceae*	Anticancer, Antioxidant, sedative, Antiviral	Rejected

S.N.	Name of the Molecules	Structure	Biological Source	Activities	Lipinski rule
5	6'-O-Trans-para-coumaroylgeniposidic Acid	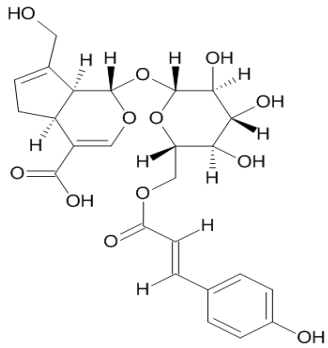	*Rubiaceae*	Anticancer, Antioxidant, sedative, Antiviral	Rejected
6	6-O-Trans-p-coumaroyl-8-O-acetylshanzhiside methyl ester	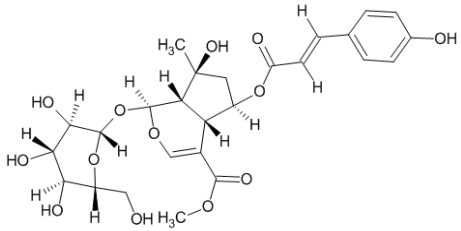	*Acanthaceae*	Antiviral, Anticancer	Rejected
7	7-Hydroxy eucommiol	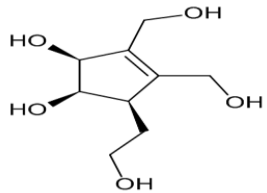	*Bignoniaceae*	Antioxidant, Anti-inflammatory	Accepted
8	8-Epideoxyloganic acid	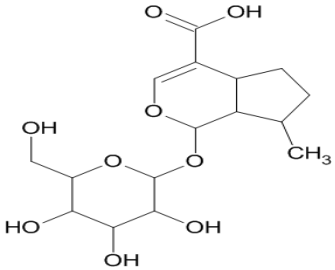	*Bigononiaceae*	Analgesia, homeostasis and anti-inflammatory	Accepted

S.N.	Name of the Molecules	Structure	Biological Source	Activities	Lipinski rule
9	8-P-coumaroylharpagide	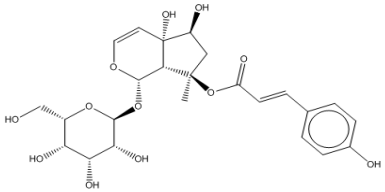	*Scrophulariaceae*	Anti-inflammatory, Antioxidant, anticancer, Antiviral	Rejected
10	10-Isovaleroyl-dihydropenstemide	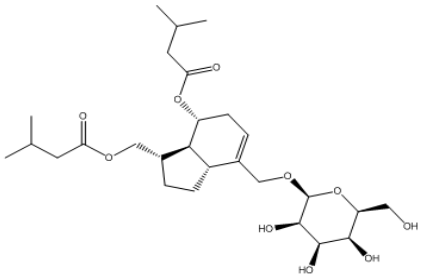	*Loganiaceae*	Anti- inflammatory, Hepatoprotective, neuroprotective, Anticancer, Anti diabetic	Accepted
11	10-O-Acetylgeniposide	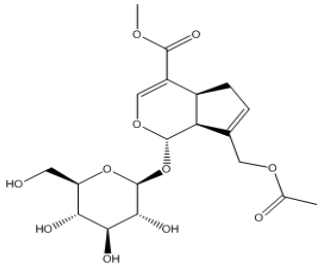	*Rubiaceae*	Anti-inflammatory, Hepatoprotective, neuroprotective, Anti - inflammatory, Anti diabetic	Accepted
12	10-O-Succinoylgeniposide	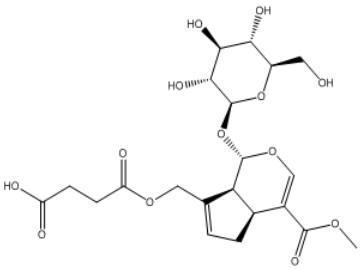	*Rubiaceae*	Cardiovascular, Anti-inflammatory, Hepatoprotective, Anti diabetic	Accepted

S.N.	Name of the Molecules	Structure	Biological Source	Activities	Lipinski rule
13	Acetylgeniposide	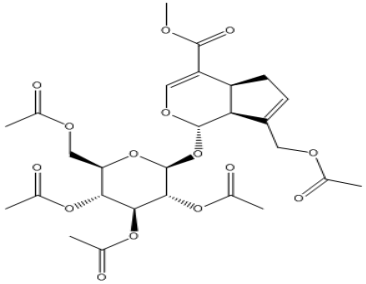	*Gardenia jasminoids*	Antii-inflammatory, Anti rheumatoid, Anti-tumor	Rejected
14	Acetylbarlerin	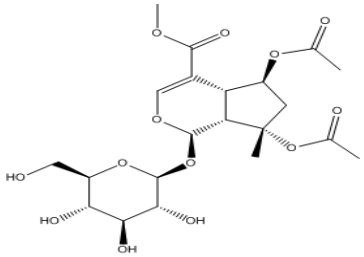	*Barlerialipulin Barleriaprionitis*	Antimicrobial, Anti-inflammatory, neuroprotective, Anti-inflammatory, Anti diabetic, Anti -cancer	Accepted
15	Amphicoside	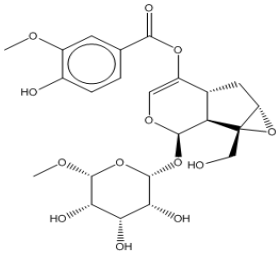	*Scrophulariaceae*	Antioxidant, anticancer	Rejected
16	Asperuloside	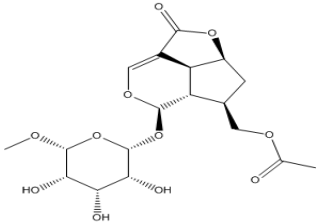	*Rubiaceae, Plantaginaceae*	Anti- melanogenesis activity	Accepted

S.N.	Name of the Molecules	Structure	Biological Source	Activities	Lipinski rule
17	Barlerin	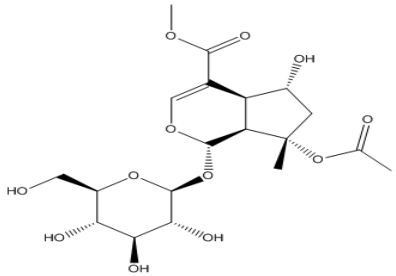	*Acanthaceae*	Antioxidant, antibacterial, anti-fungal, antidiabetic, anticancer, antiulcer	Accepted
18	Brasoside	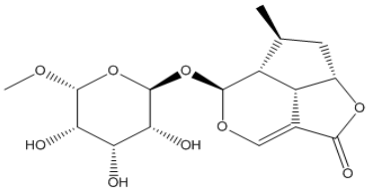	*Verbenaceae*	Antioxidant, anti-inflammatory	Accepted
19	Buddlejoside A9	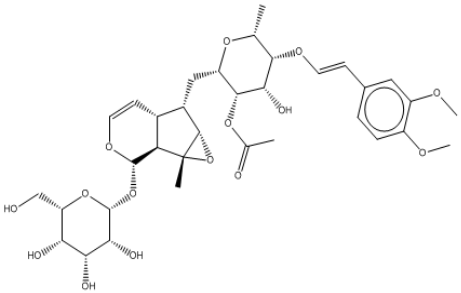	*Loganiaceae*	Antioxidant, anti-inflammatory, anticancer	Rejected
20	Cantleyoside	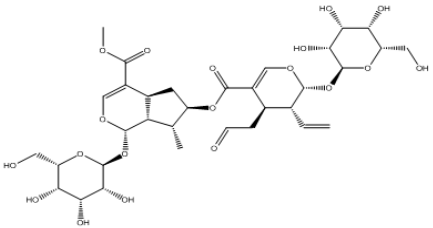	*Caprifoliaceae*	Hypoglycemic, hypolipidemic, hepatoprotective, anti-inflammatory	Rejected

S.N.	Name of the Molecules	Structure	Biological Source	Activities	Lipinski rule
21	Deacetyl asperuloside	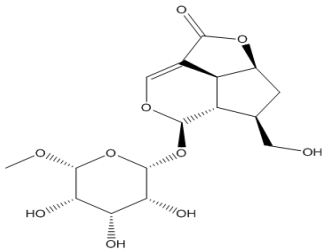	*Rubioideae*	Anti-melanogenesis activity	Accepted
22	Euphroside	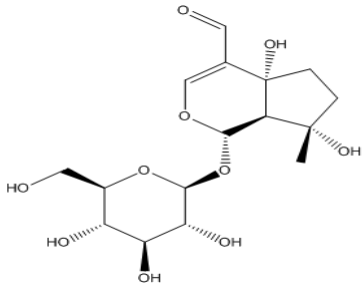	*Scrophulariaceae*	Neuroprotective, antitumor, hepatoprotective	Accepted
23	Eurostoside	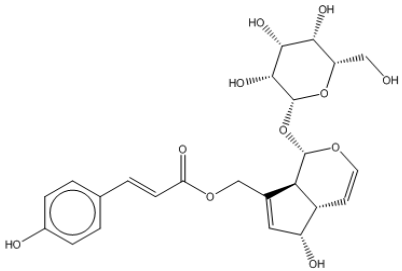	*Scrophulariaceae*	Antioxidant, anti-inflammatory, anticancer	Rejected
24	Garjasmine	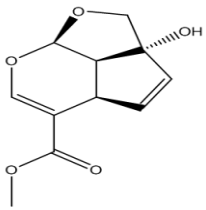	*Rubiaceae*	anticancer	Accepted

S.N.	Name of the Molecules	Structure	Biological Source	Activities	Lipinski rule
25	Geniposidic Acid	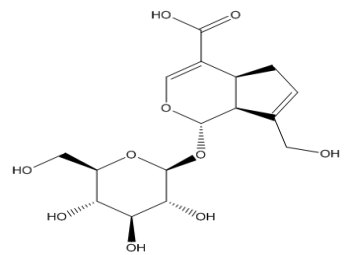	*Rubiaceae, Eucommiaceae*	Cardiovascular activity	Accepted
26	Gentiopicroside	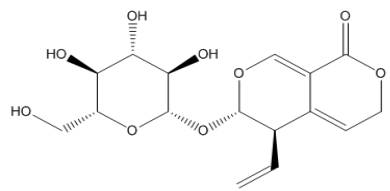	*Gentianaceae*	Digestive activity, Antioxidant hepatoprotective, anti -Inflammatory	Accepted
27	Isojaslanceoside B	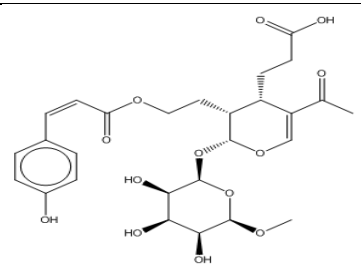	*Oleaceae*	Antioxidant hepatoprotective, anti -Inflammatory	Rejected
28	Kutkin	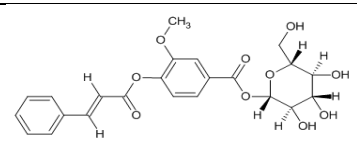	*Picrorhizakurroa*	Antioxidant hepatoprotective, anti -Inflammatory	Rejected
29	Laciniatoside I	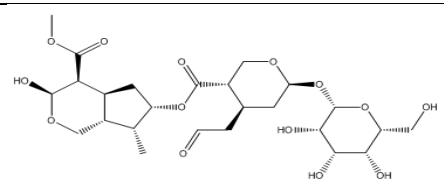	*Dipsacaceae*	Antioxidant neuroprotective, anti- inflammatory	Rejected

S.N.	Name of the Molecules	Structure	Biological Source	Activities	Lipinski rule
30	Laciniatoside II	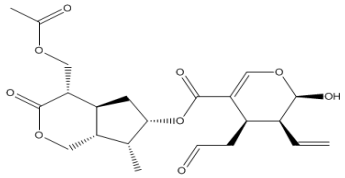	*Dipsacaceae*	Antioxidant neuroprotective, anti inflammatory	Rejected
31	Loganic acid	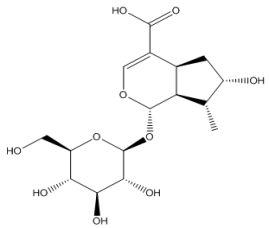	*Acanthaceae*	Anti-inflammatory, strong free radical scavenging activity	Accepted
32	Loganic acid 6'-O-beta-D-glucoside	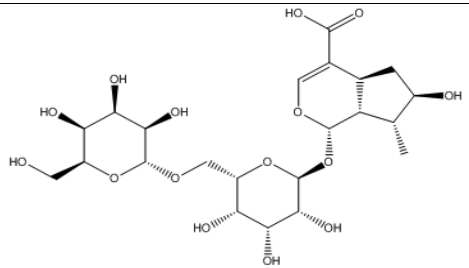	*Acanthaceae*	Anti-inflammatory, strong free radical scavenging activity	Rejected
33	Minecoside	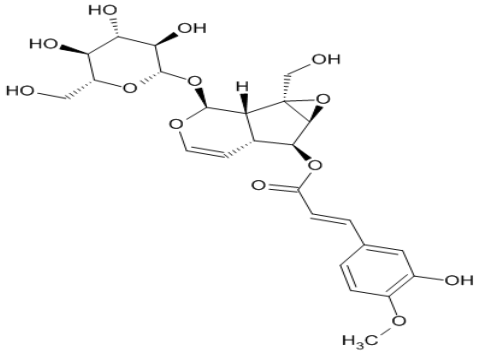	*Veronica lavaudiana.*	Antioxidant, anti-inflammatory, anticancer	Rejected

S.N.	Name of the Molecules	Structure	Biological Source	Activities	Lipinski rule
34	Mussaenoside	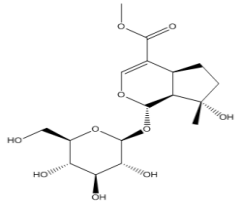	*Scrophulariaceae*	Anti inflammatory	Accepted
35	Ningpogenin	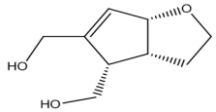	*Scrophulariaceae*	Antioxidant Neuroprotective, anti-inflammatory	Accepted
36	Nuezhenelenoliciside	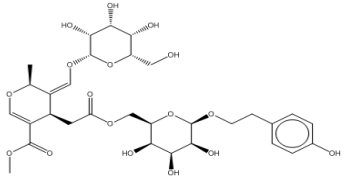	*Oleaceae*	Anti- osteoporosis activity	Rejected
37	Nuezhenide	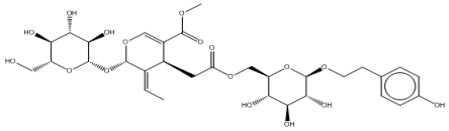	*Oleaceae*	Antibacterial, antioxidant, antitumor	Rejected
38	Oleoside dimethyl ester	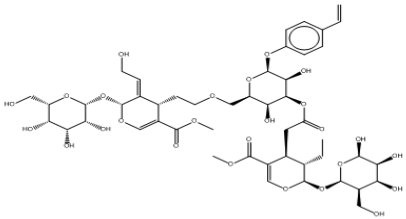	*Oleaceae*	Sedative, antioxidant	Accepted
39	Oleuropein	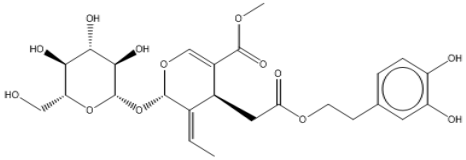	*Oleaceae*	Sedative, Anticonvulsant, antidiabetic, diuretic, antimicrobial, analgesic, antiviral	Rejected

S.N.	Name of the Molecules	Structure	Biological Source	Activities	Lipinski rule
40	Patrinalloside A	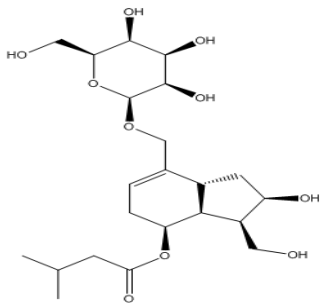	*Valerianaceae*	Antioxidant hepatoprotective, anti-inflammatory	Accepted
41	Picroside-II	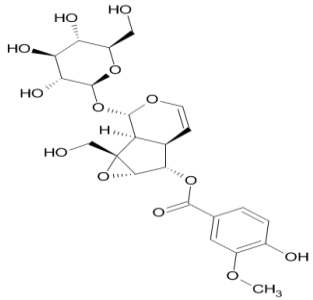	*Picrorhizakurroa*	Antioxidant hepatoprotective, anti -Inflammatory	Rejected
42	Picroside-III	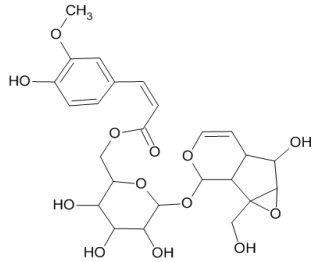	*Picrorhizakurroa*	Antioxidant hepatoprotective, anti -Inflammatory	Rejected
43	Pinnatoside	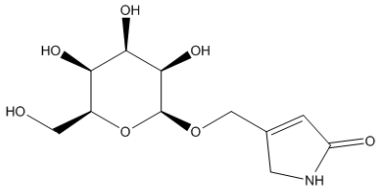	*Verbenaceae*	Antimicrobial, hepatoprotective, antioxidant	Accepted

S.N.	Name of the Molecules	Structure	Biological Source	Activities	Lipinski rule
44	Plantarenaloside	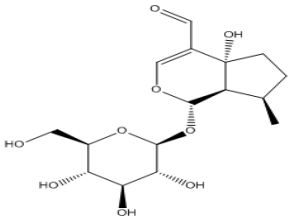	*Plantaginacea, Bigoniaceae*	Antioxidant, anti-inflammatory	Accepted
45	Polystachyn A	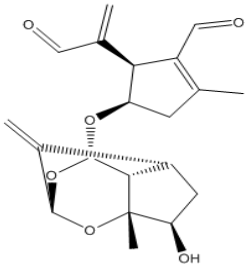	*Valerianaceae*	Antioxidant, anti-proliferative	Accepted
46	Shanzhiside methyl ester	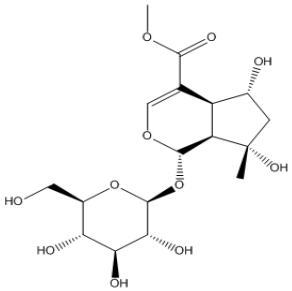	*Lamiacea*	Antimicrobial	Rejected
47	Specioside	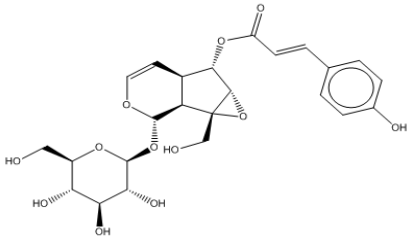	*Bignoniaceae*	Analgesic, liver stimulating	Rejected

S.N.	Name of the Molecules	Structure	Biological Source	Activities	Lipinski rule
48	Sylvestroside I	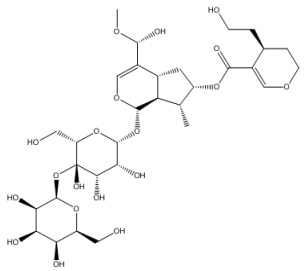	*Dipsacaceae*	Antioxidant neuroprotective, anti-inflammatory	Rejected
49	Sylvestroside III	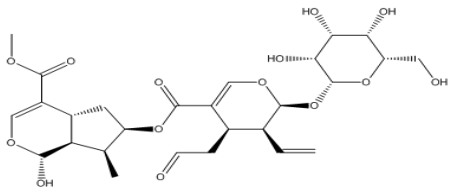	*Dipsacaceae*	Antioxidant neuroprotective, anti-inflammatory	Rejected
50	Sylvestroside III dimethyl acetal	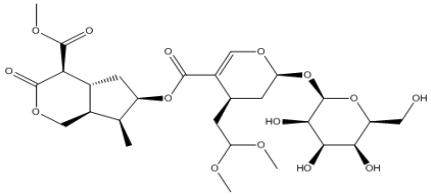	*Dipsacaceae*	Antioxidant neuroprotective, anti-inflammatory	Rejected
51	Sylvestroside IV	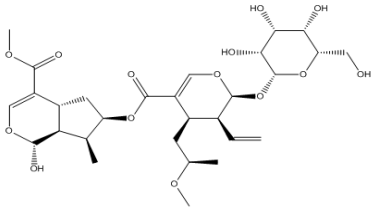	*Dipsacaceae*	Antioxidant neuroprotective, anti-inflammatory	Rejected
52	Verminoside	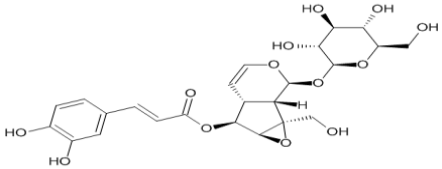	*Veronica kellereri*	Anti-inflammatory, anti-bacterial, anti-diabetic	Rejected

were conducted in a CHARMM force field environment (Kim et al. 2017). The simulations were performed using GROMACS 20.1 software, employing TIP3 water. An energy minimization process was completed with 500,000 steps. The best-docked iridoids, 10-isovaleroyl-dihydropenstemide and Patrinalloside A were subjected to a 100 ns MD simulation. During the preparation of the protein for the simulation study involving 10-isovaleroyl-dihydropenstemide and Patrinalloside A, 18641 and 18646 water molecules, along with 4 chloride ions, were added to the system. The graphical representation of the simulation trajectories was created using Microsoft Excel (Lemkul 2018).

2.4 MMPBSA Analysis

To determine the actual binding energy of ligand-receptor interactions, we applied MMPBSA analysis (Kumari and Kumar 2014). We focused on the best-docked iridoids, specifically 10-isovaleroyl-dihydropenstemide and Patrinalloside A, utilizing the MD simulation coordinates for the MMPBSA analysis (Baker et al. 2001).

2.5 Density Functional Theory Analyses

2.5.1 Frontier Molecular Orbital (FMO) Analysis

To evaluate the electrical characteristics of specific iridoids, the Lee, Yang, and Parr's (LYP) correlation functional was used in conjunction with the B3LYP/6-31G (d,p) basis set, along with Beck's (B) three-parameter hybrid model (Sakr et al. 2022). FMO (Fragment Molecular Orbital) analysis was conducted to examine the highest occupied molecular orbital (HOMO) and the lowest unoccupied molecular orbital (LUMO). The energies of these orbitals and the energy gap between them are related to the softness, electronegativity, hardness, and electrophilicity properties of the chemical structures (Perri and Weber 2014). The GAMESS software was utilized for the FMO analysis, while WxMacMolPlt (version 7.7.3) was employed to visualize the results. The best-docked iridoids, 10-isovaleroyl-dihydropenstemide and Patrinalloside A were chosen for frontier orbital analysis (Barca et al. 2020).

Chemical Hardness: $n = \frac{(I-A)}{2}$; Electronegativity: $\mu = -\frac{(I-A)}{2}$;

Electrophilicity index: $\psi = \frac{\mu 2}{2n}$; Softness: $S = \frac{1}{2n}$

where A and I are electron affinity and ionization potential. $A = -E_{LUMO}$ and $I = -E_{HOMO}$.

2.5.2 Molecular Electrostatic Potential (MEP) Analysis

The MEP (Molecular Electrostatic Potential) map focuses on the distribution of positive and negative charges within a structure. This potential map displays different colour regions: blue, green, yellow, orange, and red. The red region indicates the most negative area, where electrophiles can readily attack, while the blue region represents the most positive area for nucleophilic attacks. The green region signifies non-interacting zones, indicating areas with no potential interactions. In this analysis, the best-docked iridoids, 10-isovaleroyl-dihydropenstemide and Patrinalloside A were selected for frontier orbital analysis. The GAMESS software (version R2, released on June 30, 2024) was used alongside the B3LYP/6-31G(d,p) basis set to perform the MEP analysis (Hanson et al. 2013).

2.6 ADMET Analysis

The ADME (Absorption, Distribution, Metabolism, and Excretion) and toxicity properties of the best-docked iridoids, 10-isovaleroyl-dihydropenstemide and Patrinalloside A, were calculated using the Swiss ADME portal and OSIRIS software, respectively.

3 Results and Discussion

3.1 Molecular Docking Study Data

Inside the receptor, the ligand itraconazole was complexed with several amino acids, including PHE 25, ALA 29, PHE 28, VAL 94, TYR 95, and others represented as PRO 188 through THR 272. The Ramachandran plot of the receptor showed that 93.4% of residues were in the most favoured regions, 5.8% in the additional allowed regions, 0.3% in the generously allowed regions, and 0.5% in the disallowed regions (Riyaphan et al. 2021) (Figure 1). The overall quality value of the receptor, as per ERRAT, was 94.749, indicating good resolution (Park et al. 2023). According to the Verify3D server, 83.07% of the residues had an average 3D-1D score greater than 0.1, confirming that the amino acids present in the receptor constitute a high-quality protein for modelling (Kalman and Ben-Tal 2010).

Molecular docking interaction data showed that the docking scores of selected iridoids fluctuated between -5.5 and -8.9 kcal/mol (Ahmed et al. 2023). Voriconazole was used as a standard in this analysis, with a docking score of -7.6 kcal/mol (Table 2) (Lokhande et al. 2022). Among the tested iridoids, 10-isovaleroyl-dihydropenstemide and Patrinalloside A exhibited the highest docking scores of -8.9 kcal/mol and -8.6 kcal/mol, respectively (Paggi et al. 2024). Specifically, 10-isovaleroyl-dihydropenstemide interacted with the *N. fowleri* CYP51 receptor through hydrophobic interactions with residues TYR 82, PHE 89, and VAL 94, and via hydrogen bond interactions with ARG 338, HIS 403, and CYS 405. Patrinalloside A interacted with the receptor using hydrophobic interactions with PHE 25, PHE 28, PRO 188, LEU 189, TYR 82, ILE 334, and PHE 191, as well as a hydrogen bond interaction with MET 335 (Kumar et al. 2023). Voriconazole interacted with the receptor through hydrogen bonds with TYR 82, TYR 95, and ARG338 (Figure 2) (Kar et al. 2024).

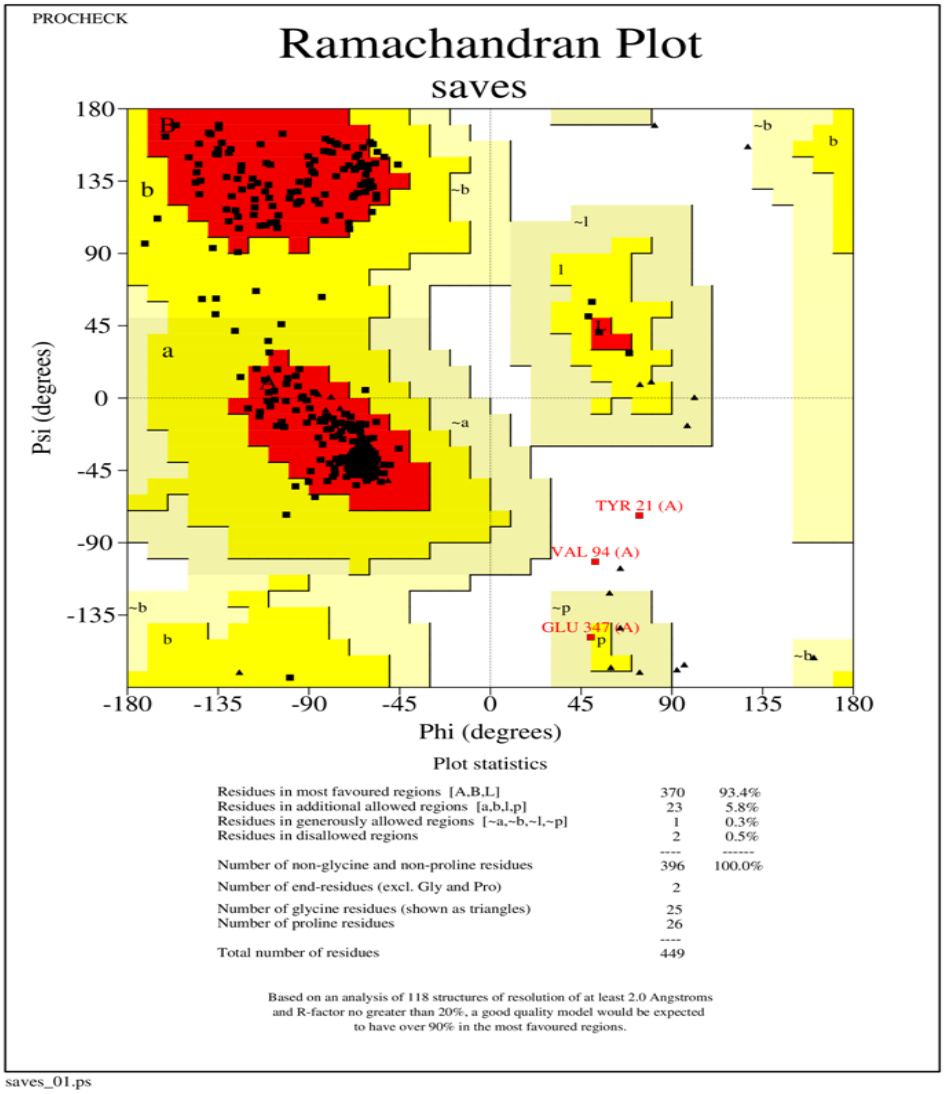

Figure 1 Ramachandran plot of 6AYC receptor

Table 2 Molecular docking interactions between iridoids and *N. fowleri* CYP51 receptor

S. N.	Name	Dock score (kcal/mol)	Hydrophobic Interactions	Hydrogen bond Interactions
1.	7-Hydroxy eucommiol	-5.5	LEU 442 (distance between interaction carbon atoms 3.57 Å).	TYR 439 (distance H-A 2.28 Å, D-A 2.83 Å), LEU442 (distance H-A 2.12 Å, D-A 3.00 Å).
2.	8-Epideoxyloganic acid	-7.8	TYR 82 (distance between interaction carbon atoms 3.43 Å), TYR 95 (distance between interaction carbon atoms 3.73 Å), LEU 442 (distance between interaction carbon atoms 3.71Å).	TYR 82 (distance H-A 2.49Å, D-A 2.93 Å), TYR95 (distance H-A 2.40 Å, D-A 3.08 Å), ILE 334 (distance H-A 2.87, D-A 3.33 Å), MET 335 (distance H-A 2.37 Å, D-A 3.26 Å).
3.	10-Isovaleroyl-dihydropenstemide	-8.9	TYR 82 (distance between interaction carbon atoms 3.72Å), PHE 89 (distance between interaction carbon atoms 3.90Å), VAL 94 (distance between interaction carbon atoms 3.69Å), VAL107 (distance between interaction carbon atoms 3.80Å), VAL110 (distance between interaction carbon atoms 3.65Å).	ARG 338 (distance H-A 2.44Å, D-A 3.13 Å), HIS 403 (distance H-A 3.17Å, D-A 3.57 Å), CYS 405 3.73 Å.

S. N.	Name	Dock score (kcal/mol)	Hydrophobic Interactions	Hydrogen bond Interactions
4.	10-O-Acetylgeniposide	-8.2	TYR 82 (distance between interaction carbon atoms 3.50Å), PHE 89 (distance between interaction carbon atoms 3.79Å), TYR 95 (distance between interaction carbon atoms 3.42Å).	TYR 82 (distance H-A 2.51Å, D-A 2.96 Å), HIS 403 (distance H-A 2.30Å, D-A 3.07 Å).
5.	10-O-Succinoylgeniposide	-8.3	PHE 89 (distance between interaction carbon atoms 3.82Å), VAL94 (distance between interaction carbon atoms 3.70Å), ALA 264 (distance between interaction carbon atoms 3.70Å), ALA268 (distance between interaction carbon atoms 3.96Å), LEU 333 (distance between interaction carbon atoms 3.63Å).	TYR 82 (distance H-A 2.37 Å, D-A 2.85 Å), HIS 403 (distance H-A 2.82Å, D-A 3.24Å), CYS 405 (distance H-A 2.72 Å, D-A 3.07 Å).
6.	Acetylbarlerin	-7.7	LYS 30 (distance between interaction carbon atoms 3.58Å).	ALA 29 (distance H-A 2.72 Å, D-A 3.13 Å).
7.	Asperuloside	-8.0	VAL 94 (distance between interaction carbon atoms 3.61Å), VAL 107 (distance between interaction carbon atoms 3.52Å), ALA 268 (distance between interaction carbon atoms 3.36Å).	TYR 82 (distance H-A 2.85 Å, D-A 3.17 Å), PHE 398 (distance H-A 2.57 Å, D-A 3.05 Å), ILE 406 (distance H-A 2.10 Å, D-A 3.10 Å).
8.	Barlerin	-7.9	ALA 150 (distance between interaction carbon atoms 3.77Å).	ASP 184 (distance H-A 3.31 Å, D-A 3.75 Å), ILE 186 (distance H-A 3.03 Å, D-A 3.62 Å), SER441 (distance H-A 3.53 Å, D-A 3.98 Å), LEU 442 (distance H-A 2.86 Å, D-A 3.65 Å).
9.	Brasoside	-8.2	TYR 82 (distance between interaction carbon atoms 3.65Å), LEU 333 (distance between interaction carbon atoms 3.56 Å).	PHE 398 (distance H-A 2.27 Å, D-A 3.04 Å), HIS 403 (distance H-A 2.32 Å, D-A 2.79 Å), CYS 405 (distance H-A 2.92 Å, D-A 3.29 Å).
10	Deacetyl asperuloside	-7.6	VAL 94 (distance between interaction carbon atoms 3.39Å), VAL 107 (distance between interaction carbon atoms 3.58 Å), ALA 268 (distance between interaction carbon atoms 3.34Å).	TYR 82 (distance H-A 2.96 Å, D-A 3.26 Å), PHE 398 (distance H-A 2.46 Å, D-A 3.13 Å).
11.	Euphroside	-7.2	ILE 275 (distance between interaction carbon atoms 3.81Å).	ASP 184 (distance H-A 3.08 Å, D-A 3.75 Å), ILE 186 (distance H-A 2.47 Å, D-A 3.00 Å), HIS 271 (distance H-A 2.36 Å, D-A 2.84 Å), SER 441 (distance H-A 2.05 Å, D-A 2.93 Å), LEU 442 (distance H-A 3.14 Å, D-A 4.09 Å), VAL 443 (distance H-A 2.34 Å, D-A 2.83Å) GLY 445 (distance H-A 2.61 Å, D-A 3.02 Å).
12.	Garjasmine	-6.5	PHE 28 (distance between interaction carbon atoms 3.83Å), PRO 32 (distance between interaction carbon atoms 3.91Å), PRO 188 (distance between interaction carbon atoms 3.5Å).	None
13.	Geniposidic Acid	-7.4	ALA 146 (distance between interaction carbon atoms 3.24Å), ILE 275 (distance between interaction carbon atoms 3.21Å).	ALA 146 (distance H-A 2.02 Å, D-A 2.70 Å), ALA 150 (distance H-A 3.31 Å, D-A 3.74 Å), ASP 183 (distance H-A 2.23 Å, D-A 2.96 Å), ASP 184 (distance H-A 2.02 Å, D-A 2.95 Å), SER 278 (distance H-A 2.24Å, D-A 3.02 Å), SER 441 (distance H-A 2.54 Å, D-A 3.43 Å), VAL 443 (distance H-A 3.06 Å, D-A 3.70 Å), GLY (distance H-A 2.13 Å, D-A 2.93 Å).

S. N.	Name	Dock score (kcal/mol)	Hydrophobic Interactions	Hydrogen bond Interactions
14.	Gentiopicroside	-7.5	TYR 82 (distance between interaction carbon atoms 3.57Å), TYR 95 (distance between interaction carbon atoms 3.91Å), LEU 333 (distance between interaction carbon atoms 3.51Å).	ARG 338 (distance H-A 2.70 Å, D-A 3.31 Å), HIS 403 (distance H-A 2.30 Å, D-A 3.14 Å).
15.	Loganic acid	-7.6	TYR 82 (distance between interaction carbon atoms 4.00Å), LEU 333 (distance between interaction carbon atoms 3.26Å), ILE 336 (distance between interaction carbon atoms 3.81Å).	TYR 82 (distance H-A 2.35 Å, D-A 2.70 Å), CYS 405 (distance H-A 2.79 Å, D-A 3.16 Å).
16.	Mussaenoside	-7.6	TYR 82 (distance between interaction carbon atoms 3.65Å), PHE 89 (distance between interaction carbon atoms 3.67Å), TYR 95 (distance between interaction carbon atoms 3.52Å).	TYR 82 (distance H-A 2.58 Å, D-A 2.98 Å), MET 335 (distance H-A 3.53 Å, D-A 3.89 Å), PHE 398 (distance H-A 2.59 Å, D-A 3.00 Å), HIS 403 (distance H-A 3.48 Å, D-A 3.96 Å), CYS 405 (distance H-A 2.82 Å, D-A 3.16 Å).
17.	Ningpogenin	-5.7	PHE 28 (distance between interaction carbon atoms 3.82Å), PRO 188 (distance between interaction carbon atoms 3.81Å), ILE 334 (distance between interaction carbon atoms 3.78Å).	None
18.	Oleoside dimethyl ester	-7.5	TYR 95 (distance between interaction carbon atoms 3.62Å), PHE 191 (distance between interaction carbon atoms 3.47Å), LEU 333 (distance between interaction carbon atoms 3.15Å), ILE 336 (distance between interaction carbon atoms 3.38Å), ILE 406 (distance between interaction carbon atoms 3.59Å), LEU 442 (distance between interaction carbon atoms 3.94Å).	ALA 29 (distance H-A 2.51 Å, D-A 3.08 Å), TYR 95 (distance H-A 2.02 Å, D-A 2.70 Å), ILE 334 (distance H-A 2.11 Å, D-A 2.80 Å), MET 335 (distance H-A 2.27 Å, D-A 2.90Å), HIS 403 (distance H-A 2.17 Å, D-A 3.12Å).
19.	Patrinalloside A	-8.6	PHE 25 (distance between interaction carbon atoms 3.96Å), PHE 28 (distance between interaction carbon atoms 3.56Å), PRO 188 (distance between interaction carbon atoms 3.24Å), LEU 189 (distance between interaction carbon atoms 3.64Å), PHE 191 (distance between interaction carbon atoms 3.33Å), PHE 192 (distance between interaction carbon atoms 3.39Å), ILE 334 (distance between interaction carbon atoms 3.44Å).	MET 335 (distance H-A 2.35 Å, D-A 3.40 Å).
20.	Pinnatoside	-6.9	PRO 188 (distance between interaction carbon atoms 3.82Å), PHE 192 (distance between interaction carbon atoms 3.61Å).	ILE 334 (distance H-A 2.21 Å, D-A 3.13Å), MET 335 (distance H-A 3.19 Å, D-A 3.89Å), LEU 442 (distance H-A 1.96 Å, D-A 2.82Å).
21.	Plantarenaloside	-7.2	TYR 82 (distance between interaction carbon atoms 3.70Å), LEU 333 (distance between interaction carbon atoms 3.59Å).	HIS 403 (distance H-A 2.05 Å, D-A 2.91Å), LYS 404 (distance H-A 2.83Å, D-A 3.52Å), CYS 405 (distance H-A 2.72 Å, D-A 3.10 Å).
22.	Polystachyn A	-8.1	LEU 78 (distance between interaction carbon atoms 3.54Å), TYR 82 (distance between interaction carbon atoms 3.53Å), TYR 95 (distance between interaction carbon atoms 3.45Å), LEU 333 (distance between interaction carbon atoms 3.69Å), ILE 336 (distance between interaction carbon atoms 3.61Å).	TYR 82 (distance H-A 2.08 Å, D-A 2.71 Å), CYS 405 (distance H-A 3.55 Å, D-A 4.00 Å).
23.	Voriconazole	-7.6	TYR 82 (4.74 Å), LEU 333 (5.50 Å), ILE 336 (5.67 Å)	TYR 95 (distance H-A 5.69 Å), ARG 338 (distance 6.04 Å, D-A 3.38Å).

H-A= Distance between hydrogen and acceptor atom (Å); D-A= Distance between donor and acceptor atom (Å)

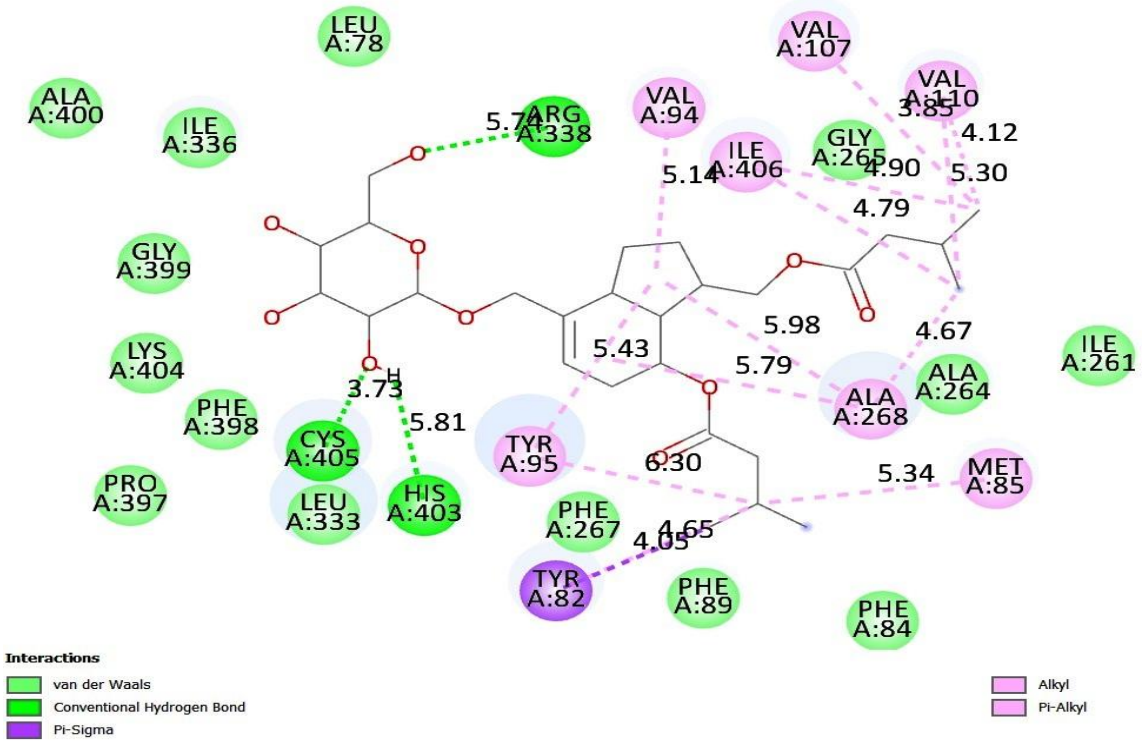

10-Isovaleroyl-dihydropenstemide

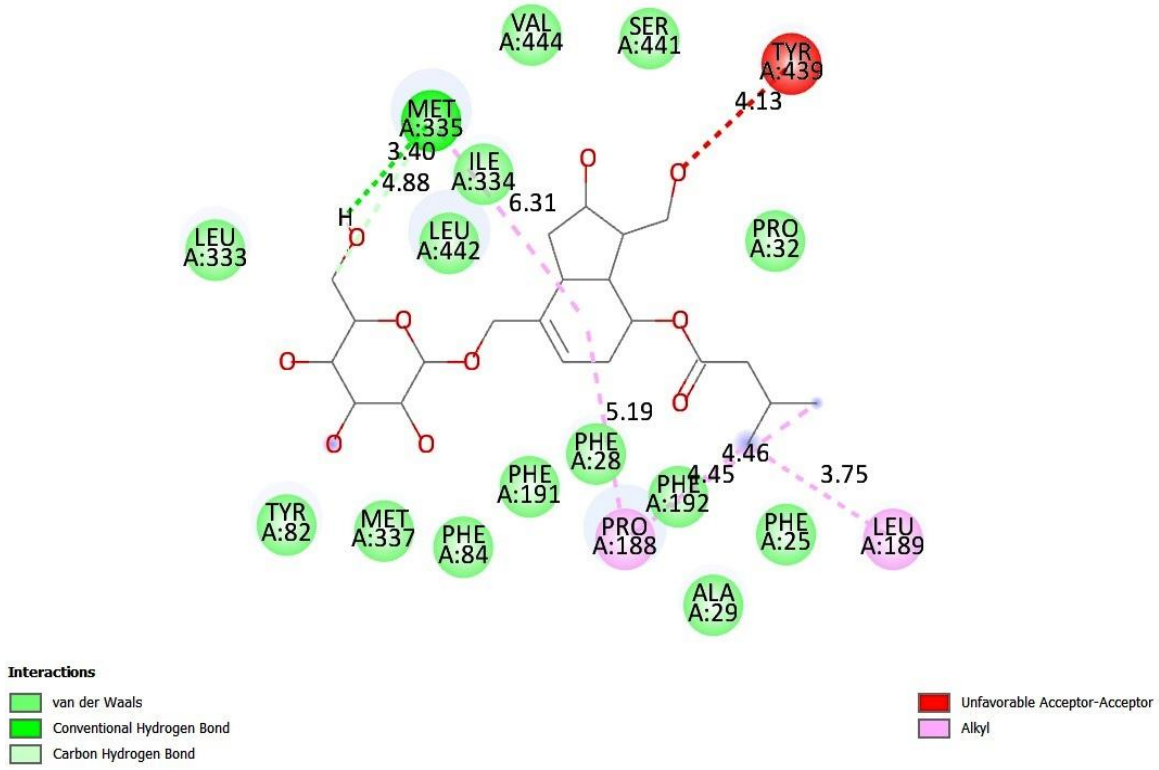

Patrinalloside A

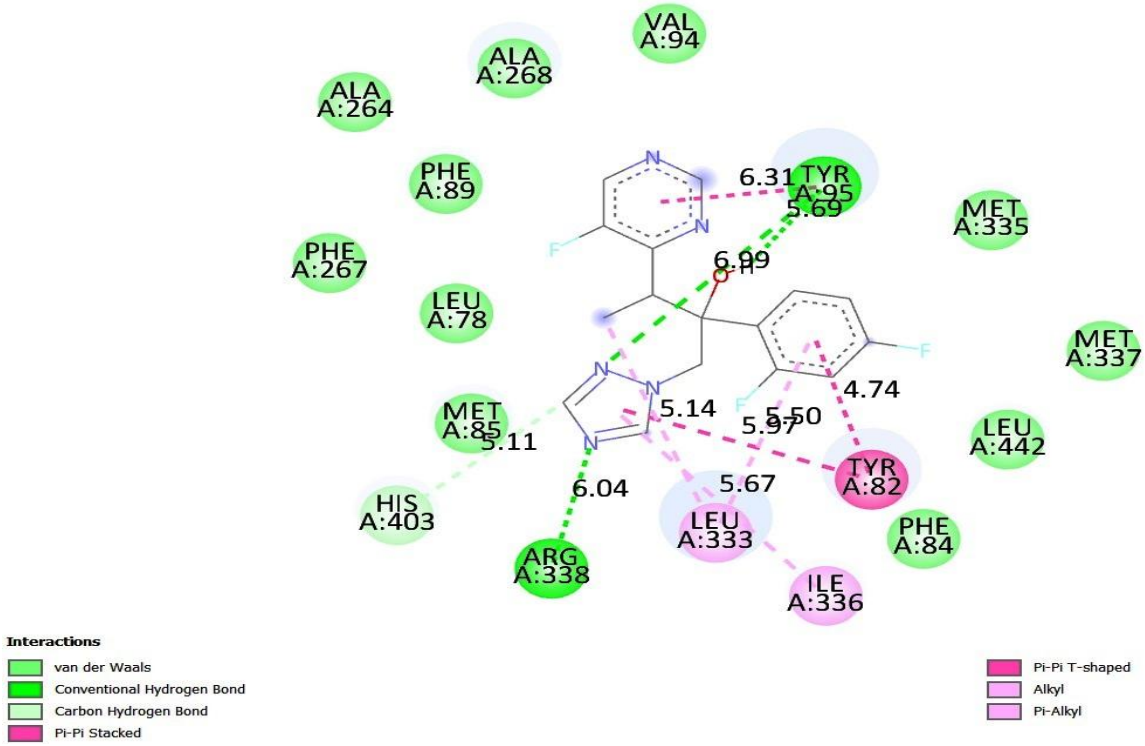

Voriconazole

Figure 2 Molecular docking interactions of 10-Isovaleroyl-dihydropenstemide, Patrinalloside A, Voriconazole with *N. fowleri*CYP51 receptor

Common amino acid residues between 10-isovaleroyl-dihydropenstemide and complexed itraconazole included VAL 94. The overlapping residues for Patrinalloside A and complexed itraconazole were PHE 25, PHE 28, PRO 188, LEU 189, PHE 191, PHE 192, and ILE 334. For voriconazole and complexed itraconazole, the common residue was TYR 95 (Madero-Ayala et al. 2022). These shared interacting residues confirmed that both 10-isovaleroyl-dihydropenstemide and Patrinalloside A were effectively docked within the active site of the receptor (Alamri et al. 2023).

3.2 MD Simulation Data

Based on molecular docking interaction data, the top two iridoids 10-isovaleroyl-dihydropenstemide and Patrinalloside A were selected for molecular dynamics simulation analysis with the *N. fowleri* CYP51 receptor (Kushwaha et al. 2021). The average RMSD (Root Mean Square Deviation) values for 10-isovaleroyl-dihydropenstemide and Patrinalloside A were 1.36 Å and 1.35 Å, respectively (Yu et al. 2024). In both cases, the RMSD values stabilized throughout the 100 ns simulation period, and both molecules maintained a similar interaction pattern during the simulation (Maharana et al. 2024). The RMSF (Root Mean Square Fluctuation) diagram showed that, for most of the simulation run, fluctuations were limited to around 2.0 Å. Inside the receptor, 10-isovaleroyl-dihydropenstemide exhibited fluctuations near residues 200, 230, and 458. Residues PRO 197, SER 234, and LYS458 showed the maximum fluctuations during the simulation, likely because they were not involved in interactions or were located far from the active site (Notarte et al. 2023). The average radius of gyration for the complexes of 10-isovaleroyl-dihydropenstemide and Patrinalloside A with the *N. fowleri* CYP51 receptor was 1.86 nm for both. Constant fluctuations were observed in the radius of gyration values; however, these values consistently remained within a lower range, confirming that the molecules were located within the receptor's active site during the simulation (Rout et al. 2024). The average solvent-accessible surface area (SASA) values for the complexes were 245.35 nm² for 10-isovaleroyl-dihydropenstemide and 244.83 nm² for Patrinalloside A. The SASA values of both complexes indicated the formation of stable structures throughout the simulation (Kokubu et al. 2024).

The hydrogen bond interaction map confirmed that both 10-isovaleroyl-dihydropenstemide and Patrinalloside A interacted with the receptor for the entire duration of the simulation. Moreover, both molecules maintained contact with the active site amino acid residues, indicating a strong relationship between the ligand and receptor (Figure 3) (Prinsa et al. 2024). The MD simulation data confirmed that both iridoids were effectively interacting with the receptor, and the structural integrity of the receptor remained intact.

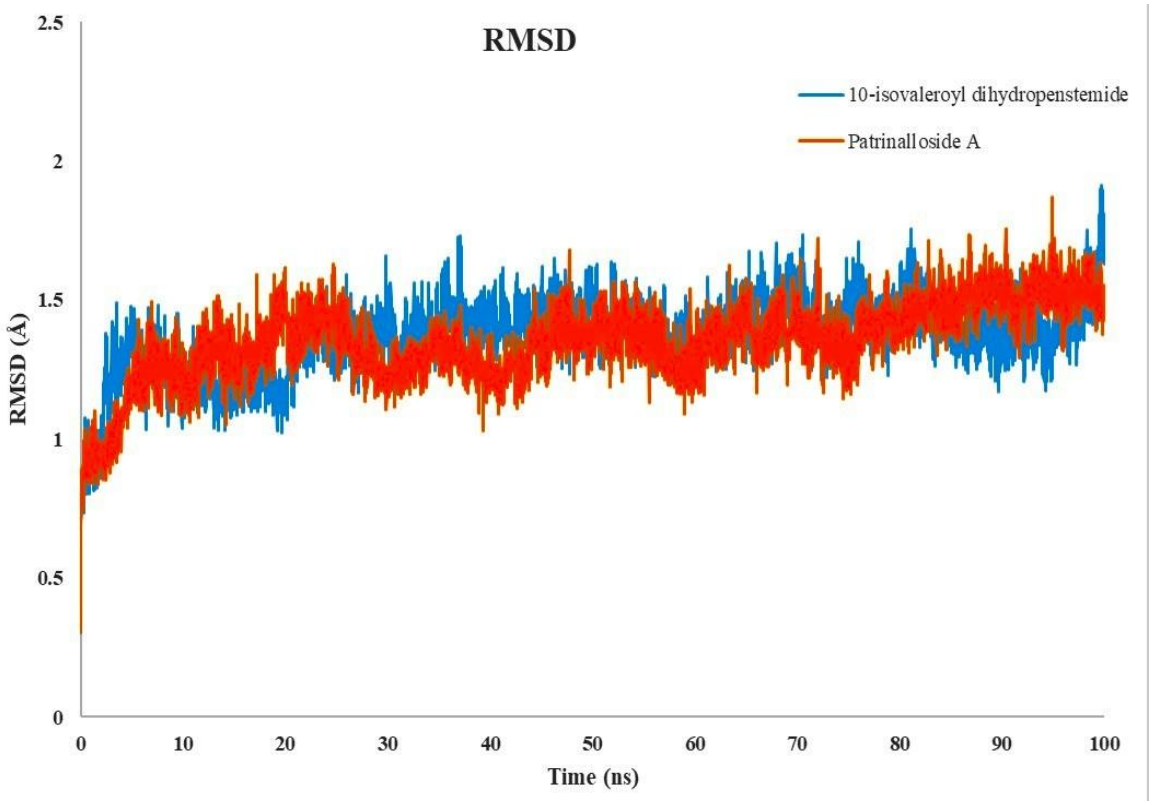
RMSD
10-isovaleroyl dihydropenstemide
Patrinalloside A
RMSD (Å)
Time (ns)
0
0.5
1
1.5
2
2.5
0
10
20
30
40
50
60
70
80
90
100

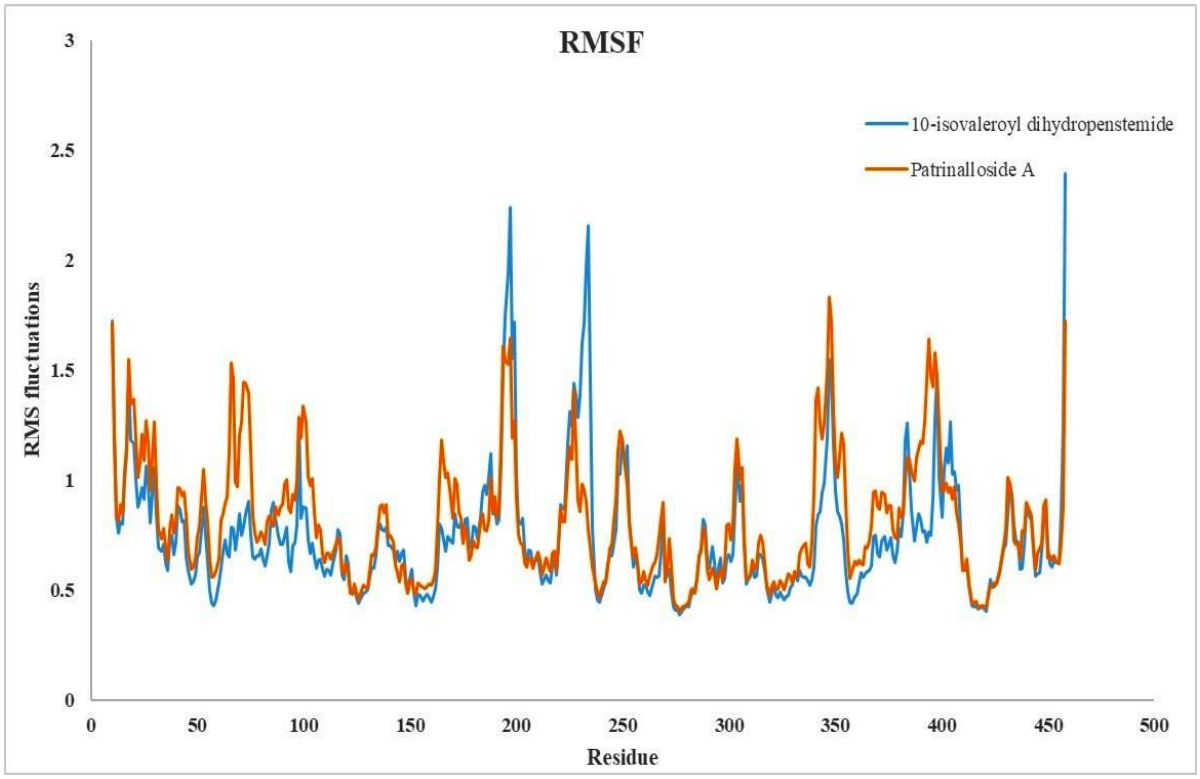
RMSF
10-isovaleroyl dihydropenstemide
Patrinalloside A
RMS fluctuations
Residue
0
0.5
1
1.5
2
2.5
3
0
50
100
150
200
250
300
350
400
450
500

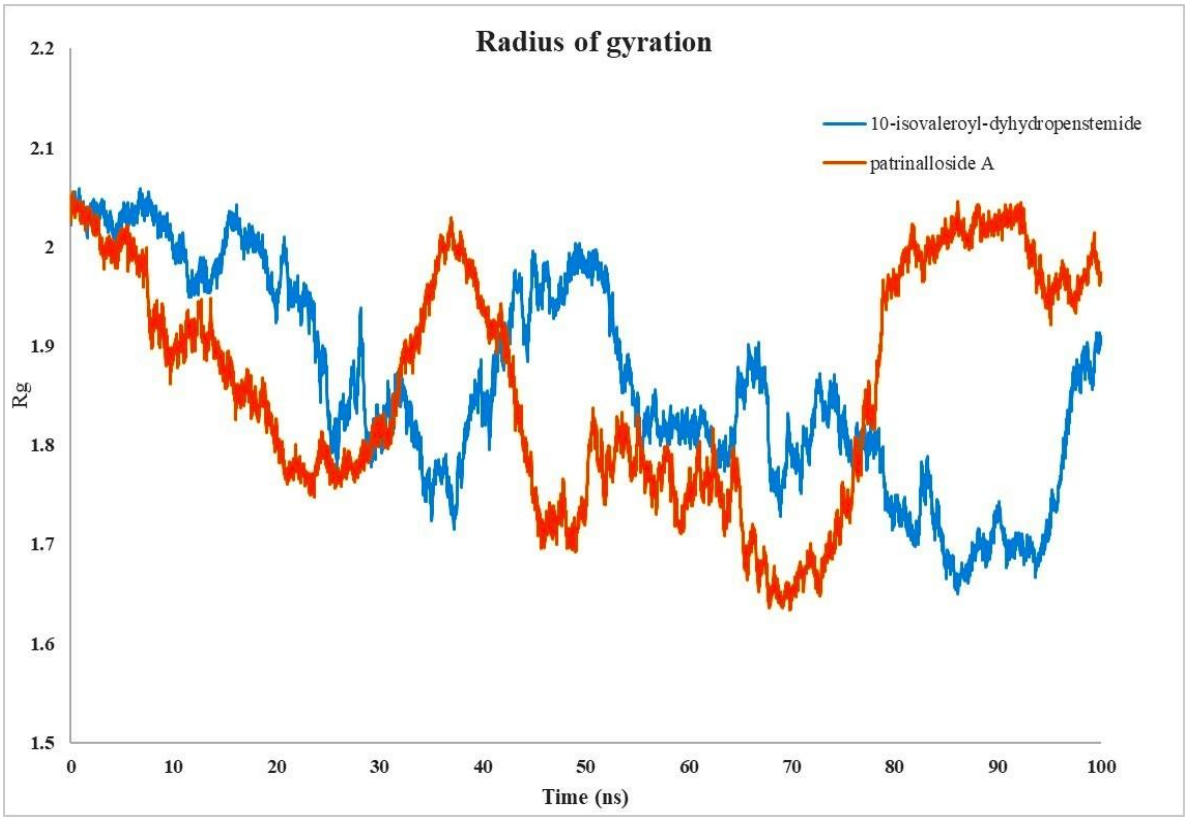
Radius of gyration
10-isovaleroyl-dyhydropenstemide
patrinalloside A
Rg
2.2
2.1
2
1.9
1.8
1.7
1.6
1.5
0
10
20
30
40
50
60
70
80
90
100
Time (ns)

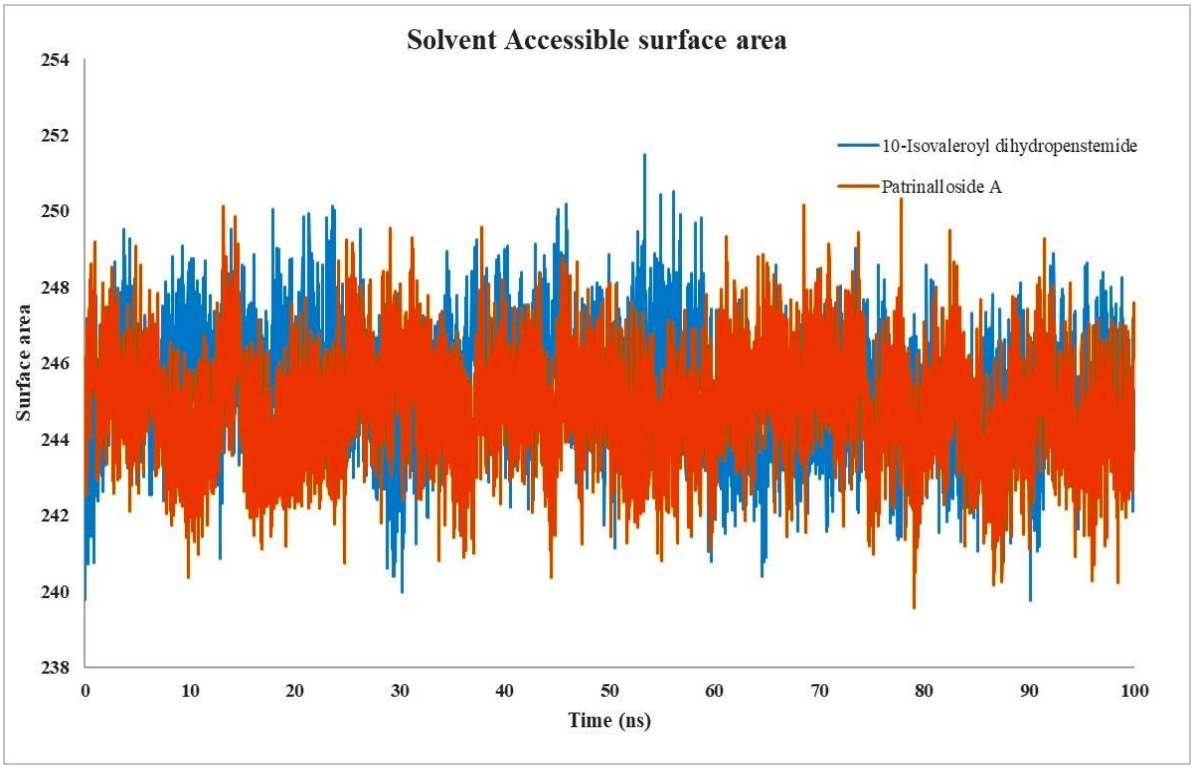
Solvent Accessible surface area
10-Isovaleroyl dihydropenstemide
Patrinalloside A
Surface area
254
252
250
248
246
244
242
240
238
0
10
20
30
40
50
60
70
80
90
100
Time (ns)

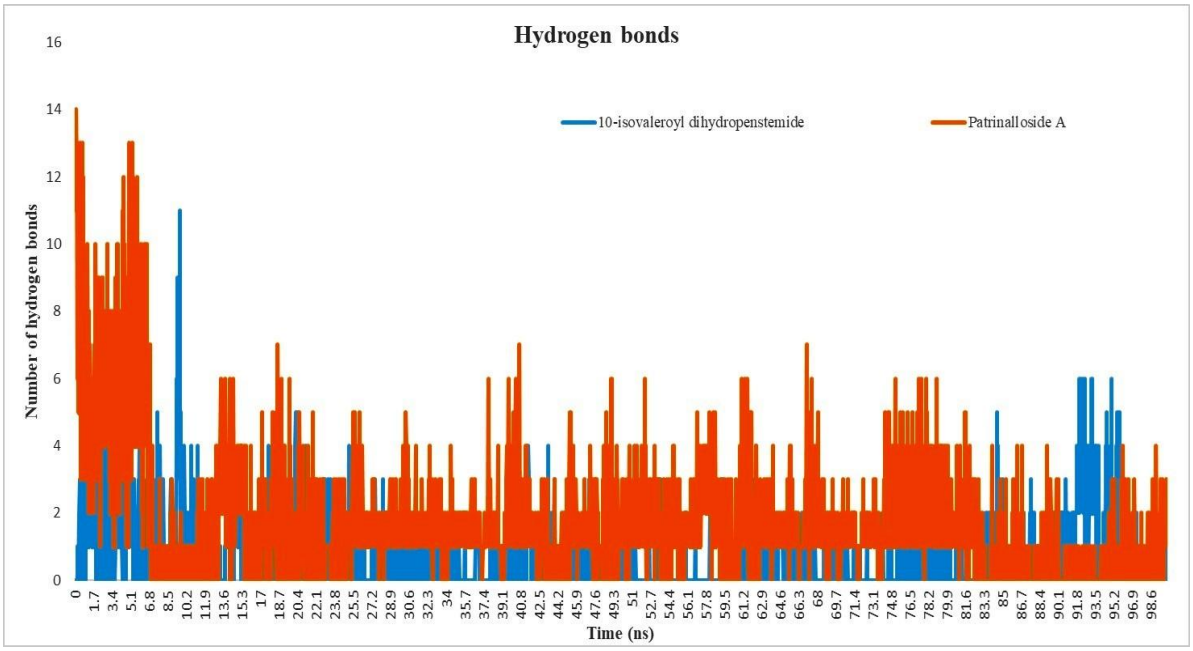

Figure 3 MD Simulation data of 10-Isovaleroyl-dihydropenstemide, and Patrinalloside Awith *N. fowleri*CYP51 receptor

Table 3 MMPBSA Data of 10-isovaleroyl-dihydropenstemide-*N.fowleri*CYP51 and Patrinalloside A -*N. fowleri* CYP51

SN	Drug-Receptor Complex	van der Waal energy (kJ/mol)	Electrostatic energy (kJ/mol)	Polar solvation energy (kJ/mol)	SASA energy (kJ/mol)	Binding energy (kJ/mol)
1.	10 -isovaleroyl-dihydropenstemide-*Naegleria fowleri* CYP51	-109.684	-6.854	59.098	-14.482	-71.922
2.	Patrinalloside A -*Naegleria fowleri* CYP51	-132.872	-26.165	114.990	-17.196	-61.243

3.3 MMPBSA Analysis Data

MMPBSA analysis data indicated that the binding energies of 10-isovaleroyl-dihydropenstemide with *N. fowleri* CYP51 and Patrinalloside A with *N. fowleri* CYP51 were -71.922 kJ/mol and -61.243 kJ/mol, respectively. In both complexes, van der Waals, electrostatic, and solvent-accessible surface area (SASA) energies positively contributed to the binding energies, while polar solvation energies had a negative contribution (Table 3) (Vishvakarma et al. 2022a).

For 10-isovaleroyl-dihydropenstemide, the residues PHE 25, LYS 30, ASP 184, LEU 189, TYR 193, and THR 440 positively contributed to the binding energies through molecular mechanics and apolar energy (Yasir et al. 2024). Conversely, residues VAL 26, ALA 29, ASP 184, SER 187, TYR 193, and THR 440 negatively impacted the binding energy through polar energy (Vishvakarma et al. 2022b). Similarly, for Patrinalloside A, the residues GLU 147, HIS 180, and PRO 448 positively contributed to the binding energies through molecular mechanics and apolar energy. However, GLU 147 and HIS 180 negatively affected the binding energy through polar energy (Figure 4) (Wagoner and Baker 2006).

3.4 DFT Analyses Data

3.4.1 Frontier Molecular Orbital Analysis Data

The HOMO and LUMO orbital energies (in eV) for 10-isovaleroyl-dihydropenstemide and Patrinalloside A were found to be 6.94 and -6.72, and -0.60 and -0.63, respectively. The energy gap between the HOMO and LUMO orbitals provides insight into the chemical reactivity of the structures. The HOMO and LUMO energy gaps for 10-isovaleroyl-dihydropenstemide and Patrinalloside A were measured at 6.34 and 6.09, respectively (Talimarada et al. 2022). Table 4 lists various parameters, including the electrophilicity index, softness, electronegativity, chemical hardness, and the energy gap (ΔE) between the HOMO and LUMO. Additionally, the compounds' softness, electrophilicity index, reactivity, chemical hardness, and electronegativity were analyzed (Wu et al. 2024). Among the selected iridoids, Patrinalloside A is classified as a soft molecule, followed by 10-

isovaleroyl-dihydropenstemide, as systems with smaller energy gaps are termed soft molecules (Lv et al. 2025). A higher value of the electrophilicity index indicates greater chemical reactivity. In this context, 10-isovaleroyl-dihydropenstemide exhibited the highest electrophilicity value of 4.08 (Figure 5) (Elyashberg et al. 2023).

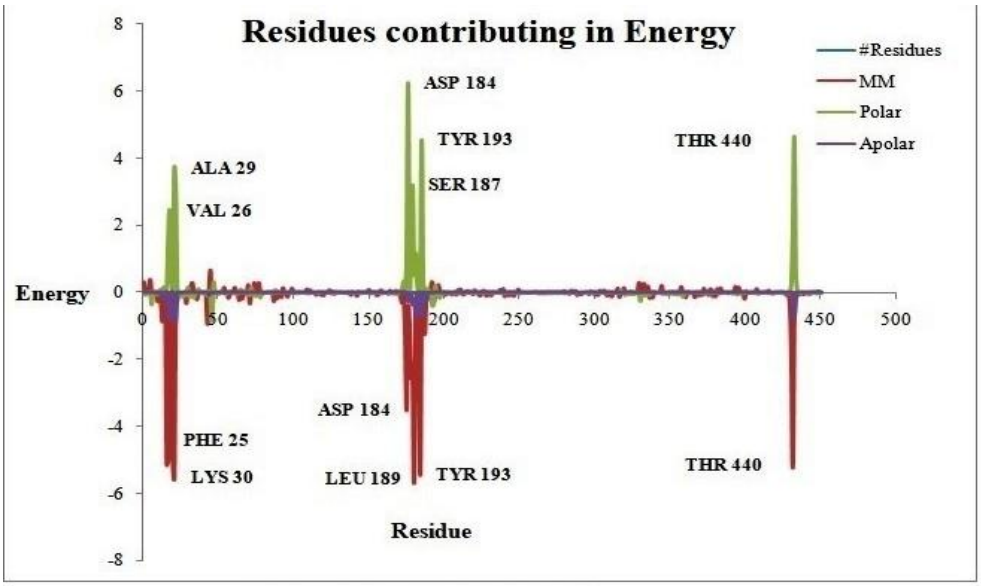

10-Isovaleroyl dihydropenstemide

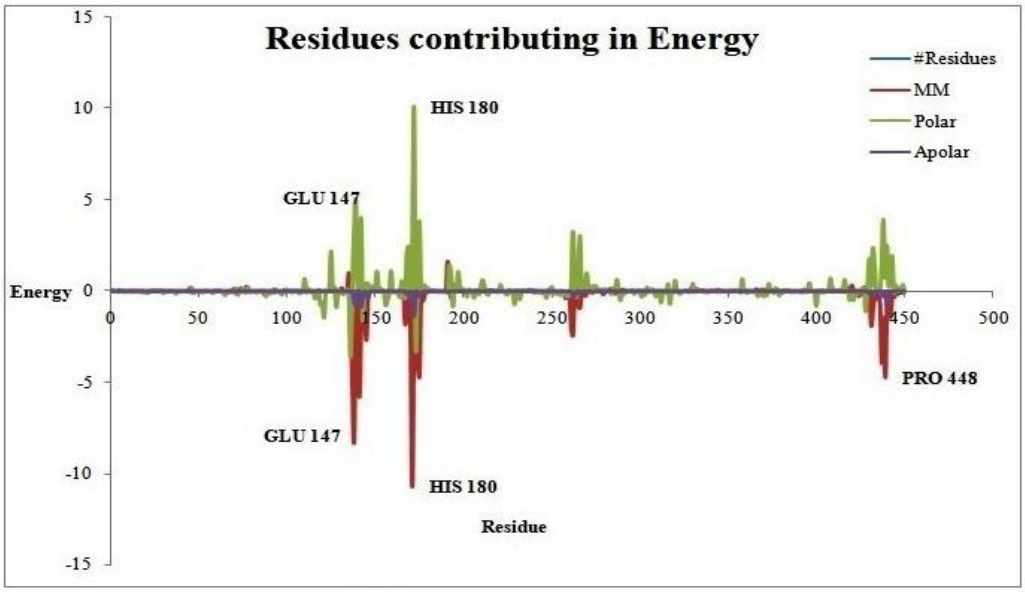

Patrinalloside A

Figure 4 Role of Amino acid residues on Binding Energy in case of 10-Isovaleroyl-dihydropenstemide, and Patrinalloside A interact with *N. fowleri* CYP51 receptor

Table 4 FMO analysis data of 10-isovaleroyl-dihydropenstemide and Patrinalloside A

SN	Molecule Name	E_{HOMO} (eV)	E_{LUMO} (eV)	ΔE gap (eV)	I	A	η	ζ	μ	Ψ
1.	10-isovaleroyl-dihydropenstemide	-6.94	-0.60	6.34	6.94	0.60	3.17	0.15	3.77	2.24
2.	Patrinalloside A	-6.72	-0.63	6.09	6.72	0.63	3.04	0.16	3.67	2.21

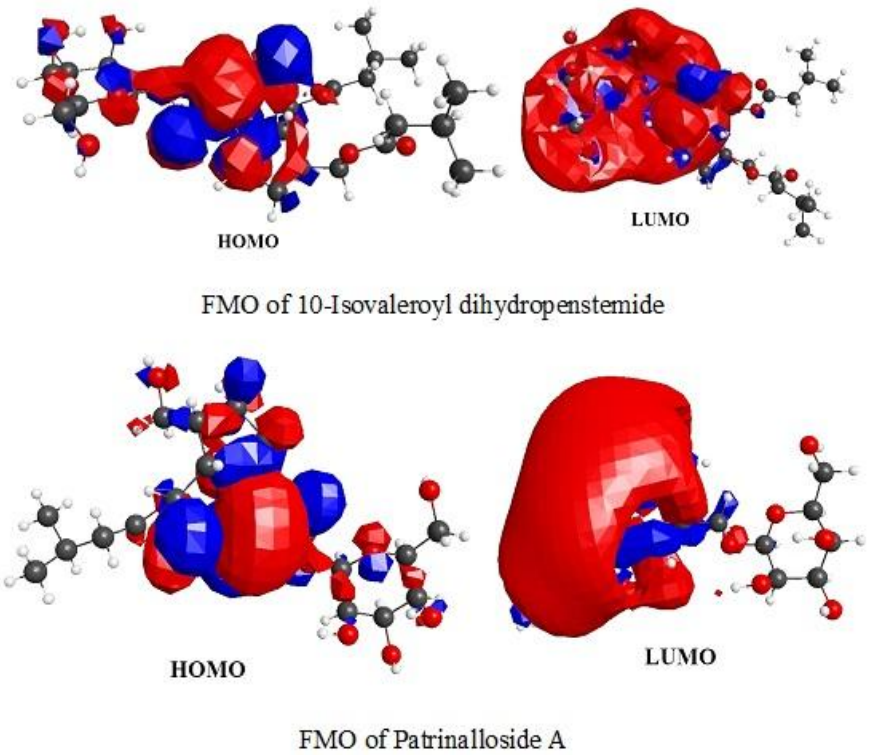

Figure 5 Frontier Molecular Orbital Analysis of 10-Isovaleroyl-dihydropenstemide, and Patrinalloside A.

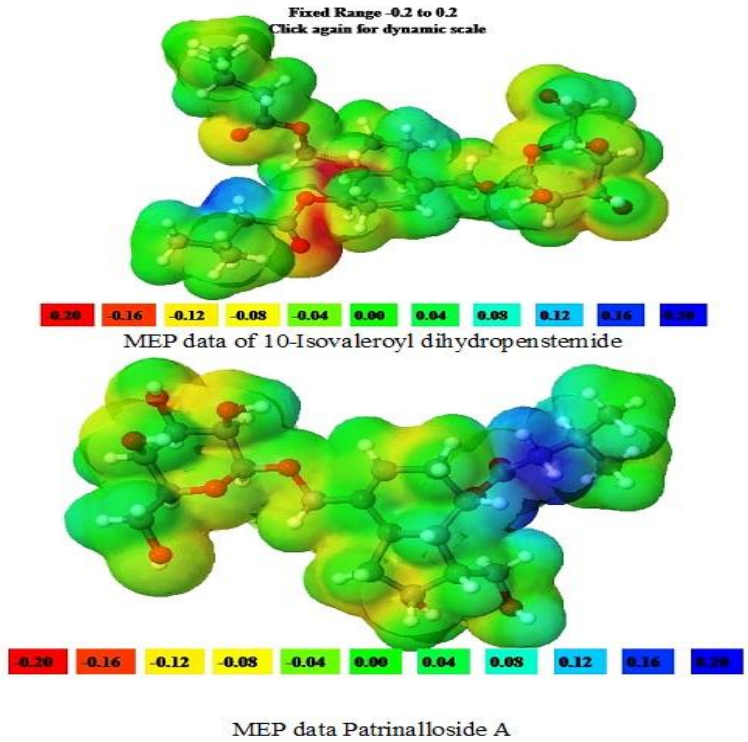

Figure 6 Molecular Orbital Potential Analysis of 10-Isovaleroyl-dihydropenstemide, and Patrinalloside A.

Table 5 ADME analysis data of 10-isovaleroyl-dihydropenstemide and Patrinalloside A

SN	Name of the Molecules	MW	TPSA	LogS	LogP	GI absorption	Molar Refractivity	Pgp substrate	BBB penetration	CYP 1A2 inhibitor	CYP 2C19 inhibitor	CYP 2C9 inhibitor	CYP 2D6 inhibitor	CYP 3A4 inhibitor
1.	10-isovaleroyl-dihydropenstemide	528.63	151.98	-3.40	4.43	Low	134.47	No	No	No	No	No	No	No
2.	Patrinalloside A	460.52	166.4	-1.70	2.69	Low	91.65	No	No	No	No	No	No	No

Table 6 OSIRIS toxicity data of 10-isovaleroyl-dihydropenstemide and Patrinalloside A

SN	Name of the Molecules	Mutagenic	Tumorigenic	Irritant	Reproductive toxicant
1.	10-isovaleroyl-dihydropenstemide	Non Toxic	Non Toxic	Non Toxic	Non Toxic
2.	Patrinalloside A	Non Toxic	Non Toxic	Toxic	Non Toxic

Toxic Non Toxic Slightly Toxic

3.4.2 Molecular Electrostatic Potential Data

In the structure of 10-isovaleroyl-dihydropenstemide, most of the compound is electrically neutral; however, the -O-C=O group and the linked methylene (-CH2-) group serve as sites for electrophilic and nucleophilic attacks, respectively (Boulebd 2025; Karakiliç et al. 2025; Saji et al. 2021). Similarly, in Patrinalloside A, the majority of the structure is electrically neutral, with the -O-C=O group acting as a site for nucleophilic attack (Figure 6) (de Souza et al. 2022).

3.5 ADMET Analysis Data

The ADME investigation of 10-isovaleroyl-dihydropenstemide and Patrinalloside A indicated that a few compounds adhered to the Lipinski rule, showing an oral bioavailability score of 0.55. However, they exhibited poor gastrointestinal absorption and did not penetrate the blood-brain barrier (Table 5). Toxicity predictions from Osiris for both 10-isovaleroyl-dihydropenstemide and Patrinalloside A demonstrated that these molecules are non-mutagenic, non-tumorigenic, and non-reproductive (Table 6) (Sultan et al. 2023).

Conclusion

In the concluding remarks, after conducting sequential computational studies, we state that among the considered iridoids, 10-isovaleroyl-dihydropenstemide and Patrinalloside A showed the highest probability of being effective in the treatment of primary amoebic meningoencephalitis.

Acknowledgement

This study is supported by Division of Research & Innovation, Uttaranchal University, Dehradun, India to Supriyo Saha under the seed money grant reference no UU/DRI/SM/2024-25/018.

Author Contributions

All authors contributed equally to the design, procurement, experiment, writing and review process of the manuscript.

References

Ahmed, U., Manzoor, M., Qureshi, S., Mazhar, M., Fatima, A., et al. (2023). Anti-amoebic effects of synthetic acridine-9(10H)-one against brain-eating amoebae. *Acta Tropica*, *239*, 106824.

Akter, S, Alhatlani, B.Y., Abdallah, E.M., Saha, S., Ferdous, J., Hossain, M.E., Ali, F., & Kawsar, S.M.A. (2023). Exploring Cinnamoyl-Substituted Mannopyranosides: Synthesis, Evaluation of Antimicrobial Properties, and Molecular Docking Studies Targeting H5N1 Influenza A Virus. *Molecules*, *28*(24), 8001.

Alamri, M.A., Alawam, A.S., Alshahrani, M.M., Kawsar, S.M.A., Prinsa., & Saha, S. (2023). Establishing the Role of Iridoids as Potential Kirsten Rat Sarcoma Viral Oncogene Homolog G12C Inhibitors Using Molecular Docking; Molecular Docking Simulation; Molecular Mechanics Poisson-Boltzmann Surface Area; Frontier Molecular Orbital Theory; Molecular Electrostatic Potential; and Absorption, Distribution, Metabolism, Excretion, and Toxicity Analysis. *Molecules*, *28*(13), 5050.

Baker, N.A., Sept, D., Joseph, S., Holst, M. J., & McCammon, J.A. (2001). Electrostatics of nanosystems: Application to microtubules and the ribosome. *Proceedings of National Academy of Science USA*, *98*, 10037-10041.

Barca, G.M.J., Bertoni, C., Carrington, L., Datta, D., De Silva, N., et al. (2020). Recent developments in the general atomic and

molecular electronic structure system. *Journal of Chemical Physics*, *152*(15), 154102.

Boulebd, H. (2025). A comprehensive DFT-based study of the antioxidant properties of monolignols: Mechanism, kinetics, and influence of physiological environments. *International Journal of Biological Macromolecule*, *284*(Pt 1), 138044.

Calis, Z, Mogulkoc, R., & Baltaci, A.K. (2020). The Roles of Flavonols/Flavonoids in Neurodegeneration and Neuroinflammation. *Mini Reviews in Medicinal Chemistry*, *20*(15), 1475-1488.

Chen, X., Li, H., Tian, L., Li, Q., Luo, J., & Zhang, Y. (2020). Analysis of the Physicochemical Properties of Acaricides Based on Lipinski's Rule of Five. *Journal of Computational Biology*, *27*(9), 1397-1406.

Cooper, A.M., Aouthmany, S., Shah, K., & Rega, P.P. (2019). Killer amoebas: Primary amoebic meningoencephalitis in a changing climate. *Journal of American Academy Physician Association*, *32*(6), 30-35.

Daina, A., Michielin, O., & Zoete, V. (2017). Swiss ADME: a free web tool to evaluate pharmacokinetics, drug-likeness and medicinal chemistry friendliness of small molecules. *Scientific Reports*, *7*, 42717.

de Souza, F.N., de Lima, H.B., de Souza, L.R., Oliveira, G.S., de Paula da Silva, C.H.T., Pereira, A.C.M., & da Silva Hage-Melim, L.I. (2022). Design of Multitarget Natural Products Analogs with Potential Anti-Alzheimer's Activity. *Current Computer Aided Drug Design*, *18*(2), 120-149.

Elyashberg, M., Tyagarajan, S., Mandal, M., & Buevich, A.V. (2023). Enhancing Efficiency of Natural Product Structure Revision: Leveraging CASE and DFT over Total Synthesis. *Molecules*, *28*(9), 3796.

Geng, X., Wang, Y., Li, H., Song, L., Luo, C., Gu, X., Zhong, H., Chen, H., Chen, X., Wang, J., & Pan, Z. (2024). Total iridoid glycoside extract of Lamiophlomis rotata (Benth) Kudo accelerates diabetic wound healing by the NRF2/COX2 axis. *Chinese Medicine*, *19*(1), 53.

Goodsell, D.S., Sanner, M.F., Olson, A.J., & Forli, S. (2021). The AutoDock suite at 30. *Protein Science*, *30*(1), 31-43.

Grover, P., Mehta, L., Malhotra, A., Kapoor, G., Nagarajan, K., Kumar, P., Chawla, V., & Chawla, P.A. (2023). Exploring the Multitarget Potential of Iridoids: Advances and Applications. *Current Topics in Medicinal Chemistry*, *23*(5), 371-388.

Güémez, A., & García, E. (2021). Primary Amoebic Meningoencephalitis by *Naegleria fowleri*: Pathogenesis and Treatments. *Biomolecules*, *11*(9), 1320.

Hanson, R.M., Prilusky, J., Renjian, Z., Nakane, T., & Sussman, J.L. (2013). JSmol and the next-generation web-based representation of 3D molecular structure as applied to proteopedia. *Israel Journal of Chemistry*, *53* (3-4), 207-216.

Hanwell, M.D., Curtis, D.E., Lonie, D.C., Vandermeersch, T., Zurek, E., & Hutchison, G.R. (2012). Avogadro: an advanced semantic chemical editor, visualization, and analysis platform. *Journal of Cheminformatics*, *4*, 17.

He, F., Yan, X., Zhao, N., Jiang, X., Wei, Y., Lu, F., Li, H., Li, D., & Chen, Y. (2023). Iridoid-glycoside isolation and purification from *Premna fulva* leaves. *Journal of Separation Science*, *46*(14), e2300059.

Kalman, M., & Ben-Tal, N. (2010). Quality assessment of protein model-structures using evolutionary conservation. *Bioinformatics*, *26*(10), 1299-307.

Kar, P., Oriola, A.O., & Oyedeji, A.O. (2024). Molecular Docking Approach for Biological Interaction of Green Synthesized Nanoparticles. *Molecules*, *29*(11), 2428.

Karakiliç, E., Başçeken, S., Eskiler, G.G., Uzuner, U., & Baran, A. (2025). Bioimaging of thiazolidine-4-one-based new probes, fluorimetric detection of Cu2+ "on-off" sensor property, DFT calculation, molecular docking studies, and multiple real samples application. *Food Chemistry*, *463*(Pt 2), 141269.

Kawsar, S.M.A., Hossain, M.A., Saha, S., Abdallah, E.M., Bhat, A.R., Ahmed, S., Jamalis, J., & Ozeki Y. (2024). Nucleoside-Based Drug Target with General Antimicrobial Screening and Specific Computational Studies against SARS-CoV-2 Main Protease. *Chemistry Select*, *9*, e202304774.

Kim, S., Lee, J., Jo, S., Brooks, C.L. 3rd., Lee, H.S., & Im, W. (2017). CHARMM-GUI ligand reader and modeler for CHARMM force field generation of small molecules. *Journal of Computational Chemistry*, *38*(21), 1879-1886.

Kokubu, R., Ohno, S., Manabe, N., & Yamaguchi, Y. (2024). Molecular Dynamics Simulation and Docking of MUC1 O-Glycopeptide. *Methods in Molecular Biology*, *2763*, 373-379.

Kumar, P., Kumar, P, Shrivastava, A., Dar, M.A., Lokhande, K.B., Singh, N., Singh, A., Velayutham, R., and Mandal, D. (2023). Immunoinformatics-based multi-epitope containing fused polypeptide vaccine design against visceral leishmaniasis with

high immunogenicity and TLR binding. *International Journal of Biological Macromolecule*, *253*(Pt 8), 127567.

Kumari, R., & Kumar, R. (2014). Open Source Drug Discovery Consortium, Lynn A. g_mmpbsa-A GROMACS Tool for High-Throughput MM-PBSA Calculations. *Journal of Chemical Information and Modeling*, *54*(7), 1951–1962.

Kushwaha, P.P., Singh, A.K., Bansal, T., Yadav, A., Prajapati, K.S., Mohd, S., & Kumar, S. (2021). Identification of Natural Inhibitors Against SARSCoV-2 Drugable Targets Using Molecular Docking, Molecular Dynamics Simulation, and MM-PBSA Approach. *Frontier Cellular Infection Microbiology*, *11*, 730288.

Lemkul, J.A. (2018). From Proteins to Perturbed Hamiltonians: A Suite of Tutorials for the GROMACS-2018 Molecular Simulation Package, v1.0. *Living Journal of Computational Molecular Science*, *1*(1) 5068.

Lokhande, K., Nawani, N.K., Venkateswara, S., & Pawar, S. (2022). Biflavonoids from *Rhus succedanea* as probable natural inhibitors against SARS-CoV-2: a molecular docking and molecular dynamics approach. *Journal of Biomolecular Structure Dynamics*, *40*(10), 4376-4388.

Lv, H., Ruan, M., Wen, Y., Zhou, L., Zhao, P., & Xuan, X. (2025). Toward understanding ammonia capture in two amino-functionalized metal-organic frameworks using in-situ infrared spectroscopy and DFT calculation. *Spectrochima Acta A Molecular and Biomolecular Spectroscopy*, *324*, 124962.

Madero-Ayala, P.A., Mares-Alejandre, R.E., & Ramos-Ibarra, M.A. (2022). In Silico Structural Analysis of Serine Carboxypeptidase Nf314, a Potential Drug Target in *Naegleria fowleri* Infections. *International Journal of Molecular Sciences*, *23*(20), 12203.

Maharana, J., Hwang, S.K., Singha, D.L., Panda, D., Singh, S., Okita, T.W., & Modi, M.K. (2024). Exploring the structural assembly of rice ADP-glucose pyrophosphorylase subunits using MD simulation. *Journal of Molecular Graphics & Modeling*, *129*, 108761.

Notarte, K.I.R., Quimque, M.T.J., Macaranas, I.T., Khan, A., Pastrana, A.M., Villaflores, O.B., et al. (2023). Attenuation of Lipopolysaccharide-induced Inflammatory Responses through Inhibition of the NF-κB Pathway and the Increased NRF2 Level by a Flavonol-enriched n-Butanol Fraction from Uvaria alba. *ACS Omega*, *8*(6), 5377–5392.

Paggi, J.M., Pandit, A., & Dror, R.O. (2024). The Art and Science of Molecular Docking. *Annual Review of Biochemistry*, *93*(1), 389-410.

Park, S.W., Lee, B.H., Song, S.H., & Kim, M.K. (2023). Revisiting the Ramachandran plot based on statistical analysis of static and dynamic characteristics of protein structures. *Journal of Structural Biology*, *215*(1), 107939.

Perri, M.J., & Weber, S.H. (2014). Web-Based Job Submission Interface for the GAMESS Computational Chemistry Program. *Journal of Chemical Education*, *91*(12), 2206-2208.

Prinsa., Saha, S., Bulbul, M.Z.H., Ozeki, Y., Alamri, M.A., & Kawsar S.M.A. (2024). Flavonoids as potential KRAS inhibitors: DFT, molecular docking, molecular dynamics simulation and ADMET analyses. *Journal of Asian Natural Product Research*, *26*(8), 955-992.

Riyaphan, J, Pham, D.C., Leong, M.K., & Weng, C.F. (2021). In Silico Approaches to Identify Polyphenol Compounds as α-Glucosidase and α-Amylase Inhibitors against Type-II Diabetes. *Biomolecules*, *11*(12), 1877.

Rojo, J.U., Rajendran, R., & Salazar, J.H. (2023). Laboratory Diagnosis of Primary Amoebic Meningoencephalitis. *Laboratory Medicine*, *54*(5), e124-e132.

Rout, M., Dey, S., Mishra, S., Panda, S., Singh, M.K., Sinha, R., Dehury, B., & Pati, S. (2024). Machine learning and classical MD simulation to identify inhibitors against the P37 envelope protein of monkeypox virus. *Journal of Biomolecular Structure & Dynamics*, *42*(8), 3935-3948.

Saji, R.S., Prasana, J.C., Muthu, S., & George, J. (2021). Experimental and theoretical spectroscopic (FT-IR, FT-Raman, UV-VIS) analysis, natural bonding orbitals and molecular docking studies on 2-bromo-6-methoxynaphthalene: A potential anticancer drug. *Heliyon*, *7*(6), e07213.

Sakr, M.A.S., Sherbiny, F.F., & El-Etrawy, A.S. (2022). Hydrazone-based Materials; DFT, TD-DFT, NBO Analysis, Fukui Function, MESP Analysis, and Solar Cell Applications. *Journal of Fluorescence*, *32*(5), 1857-1871.

Schou, C., Kolören, Z., Sendker, J., Sarigiannis, Y., Jovanovic, A., & Karanis, P. (2024). *Odontites linkii* subsp. cyprius Ethanolic Extract Indicated In Vitro Anti-Acanthamoeba Effect. *Microorganisms*, *12*(11), 2303.

Shi, D.Q., Liu, J.J., Feng, Y.M., Zhou, Y., Liao, C.C., Liu, D., Li, R.T., & Li, H.M. (2023). Iridoids and sesquiterpenoids from *Valeriana officinalis* and their bioactivities. *Phytochemistry*, *205*, 113478.

Sultan, R., Ahmed, A., Wei, L., Saeed, H., Islam, M., & Ishaq M. (2023). The anticancer potential of chemical constituents of

Moringa oleifera targeting CDK-2 inhibition in estrogen receptor positive breast cancer using in-silico and in vitro approches. *BMC Complementary Medicine and Therapies*, *23*(1), 396.

Talimarada, D., Sharma, A., Wakhradkar, M.G., Dhuri, S.N., Gunturu, K.C., Sundaram, V.N.N., & Holla, H. (2022). Synthesis, DFT analysis and in-vitro anticancer study of novel fused bicyclic pyranoneisoxazoline derivatives of Goniodiol-diacetate-a natural product derivative. *Fitoterapia*, *163*, 105316.

Vishvakarma, V.K., Pal, S., Singh, P., & Bahadur, I. (2022a). Interactions between main protease of SARS-CoV-2 and testosterone or progesterone using computational approach. *Journal of Molecular Structure*, *1251*, 131965.

Vishvakarma, V.K., Singh, M.B., Jain, P., Kumari, K., & Singh, P. (2022b). Hunting the main protease of SARS-CoV-2 by plitidepsin: Molecular docking and temperature-dependent molecular dynamics simulations. *Amino Acids*, *54*, 205–213.

Wagoner, J.A., & Baker, N.A. (2006). Assessing implicit models for nonpolar mean solvation forces: the importance of dispersion and volume terms. *Proceedings of National Academy of Science USA*, *103*(22), 8331-6.

Wang, C., Gong, X., Bo, A., Zhang, L., Zhang, M., Zang, E., Zhang, C., & Li, M. (2020). Iridoids: Research Advances in Their Phytochemistry, Biological Activities, and Pharmacokinetics. *Molecules*, *25*(2), 287.

Wu, Q., Ghosal, K., Kana'an, N., Roy, S., Rashed, N., Majumder, R., Mandal, M., Gao, L., & Farah, S. (2024). On-demand imidazolidinyl urea-based tissue-like, self-healable, and antibacterial hydrogels for infectious wound care. *Bioactive Materials*, *44*, 116-130.

Yasir, M., Park, J., Han, E.T., Han, J.H., Park, W.S., & Chun, W. (2024). Investigating the Inhibitory Potential of Flavonoids against Aldose Reductase: Insights from Molecular Docking, Dynamics Simulations, and gmx_MMPBSA Analysis. *Current Issues in Molecular Biology*, *46*(10), 11503-11518

Yu, D., Li, H., Liu, Y., Yang, X., Yang, W., Fu, Y., Zuo, Y.A., & Huang, X. (2024). Application of the molecular dynamics simulation GROMACS in food science. *Food Research International*. *190*, 114653.

Zhang, L., Wu, L., Liu, J., Chen, K., & Li, Y. (2023). Iridoids and derivatives from *Catalpa ovata* with their antioxidant activities. *Fitoterapia*, *169*, 105599.

Zhang, Q., Ran, T., Li, S., Han, L., Chen, S., Lin, G., Wu, H., Wu, H., Feng, S., Chen, J., Zhang, Q., & Zhao, X. (2024). Catalpol ameliorates liver fibrosis via inhibiting aerobic glycolysis by EphA2/FAK/Srcsignaling pathway. *Phytomedicine*. *135*, 156047.